Spatially-Resolved Spectroscopic Properties of Low-Redshift Star-Forming Galaxies

Sebastián F. Sánchez[1]

[1]Instituto de Astronomía, Universidad Nacional Autónoma de México, A. P. 70-264, C.P. 04510, México, D.F., Mexico; email: sfsanchez@astro.unam.mx

Abstract

I review here the spatially-resolved spectroscopic properties of low-redshift star-forming galaxies (and their retired counter-parts), using results from the most recent Integral Field Spectroscopy galaxy surveys. First, I briefly summarise the global spectroscopic properties of these galaxies, discussing the main ionization processes, and the global relations described between the star-formation rates, oxygen abundances, and average properties of their stellar populations (age and metallicity) with the stellar mass. Second, I present the local distribution of the ionizing processes, down to kiloparsec scales, and I show how the global scaling relations found between integrated parameters (like the star-formation main sequence, mass-metallicity relation and Schmidt-Kennicutt law) present local/resolved counter-parts, with the global ones being just integrated/average versions of the local ones. I discuss the local/resolved star-formation and chemical enrichment histories and their implication on the inside-out growth of galaxies. Third, I present the radial distributions of the surface densities of the properties explored globally, and how they depend on the integrated galaxy properties. Finally, I summarise all these results and discuss what we have learned from them regarding the evolution of galaxies.

Contents

1. INTRODUCTION

The formation of stars from gas is one the physical processes that contributes more deeply to shape our Universe. Without the ignition of the thermonuclear reactions that power stars it would be impossible to conceive our physical world. There would be basically no chemical elements besides hydrogen and helium (and traces of lithium), no complex chemical compounds, no rocky planets, and no life. Therefore, the study of the conditions required to form stars is of key importance to understand our existence. As individual entities the birth of stars is governed by detailed physical laws, and therefore, given some particular conditions of gas density, pressure and metallicity, their ignition is triggered (e.g. Bonnell et al. 1998). However, when large stellar populations are considered ($M_* \sim 10^4 M_\odot$), star-formation is regulated by rather statistical laws that correlate the main observed properties, like the neutral gas density and the star-formation rate (SFR), averaged over hundreds of parsecs or kiloparsecs scales across the galaxies (Kennicutt 1998b). In this context it is relevant to understand whether these laws are the same for all galaxy types or they depend either on local (kilo-parsec scales or the scale of molecular clouds) or general properties of the galaxies in which star-formation happens.

It is evident that all galaxies formed stars in the past and in general the star-formation rate was higher in the past both in individual galaxies (e.g. Heavens et al. 2004, Speagle et al. 2014) and averaged over the entire population (e.g. Madau & Dickinson 2014). However, at low redshift and at least up to z~1 galaxies present a clear bimodality regarding their SFR: (i) those that are more actively forming stars (defined broadly as star-forming galaxies, SFGs), and (ii) those that present little or no star-formation activity (defined broadly as passive, retired or quenched, RGs) (e.g. Stasińska et al. 2008). These two groups are well separated in different diagrams that compare either the current SFR or proxies of the age of the stellar population with the integrated stellar mass or absolute magnitude, like the SFR vs. Mass diagram (SFR-M_*, e.g. Renzini & Peng 2015), the Color-Magnitude diagram (e.g. Bell et al. 2004), or the D4000-Mass diagram (e.g. Blanton & Moustakas 2009, where D4000 is an age tracer). Even more, this bimodality is strongly correlated with the morphological, structural and

SFGs: Star forming galaxies: those that are more actively forming stars.

RGs: Retired galaxies: those that present little or no star-formation activity.

dynamical properties of the galaxies (e.g. Blanton & Moustakas 2009, Drory & Fisher 2007, Graham et al. 2018). In general, star-forming galaxies are late-type, disk dominated (e.g. Brinchmann et al. 2004), while retired galaxies are more early-type, bulge dominated (e.g. Drory & Fisher 2007). Even more, we know that the mass of early-type galaxies at low redshift have grown at least a factor two in the last ~8 Gyrs (e.g. Bell et al. 2006), although they show little or no significant star-formation during the same time period (e.g. López Fernández et al. 2018, Sánchez et al. 2019a). This implies that there should be a transition of galaxies from the star-forming to the retired galaxy population. This event may last only a few Gyr, and it involves a profound morphological and structural tranformation of those galaxies, as well as a dramatic ageing of their average stellar populations. Broadly speaking, this process is known as quenching or rapid halting of the star-formation activity (e.g. Casado et al. 2015, Saintonge et al. 2016). Beside that dramatic process, current star-forming galaxies have steadily decreased their SFR along the same time period, showing slightly older stellar populations on average, a smooth proccess generally known as aging (e.g. Casado et al. 2015).

Our understanding of nearby galaxies and their evolution has deeply improved since the advent of large imaging surveys, complemented for a lower number of objects with single-fiber spectroscopy (e.g., Sloan Digital Sky Survey, SDSS, Galaxy and Mass Assembly survey, GAMA, York et al. 2000, Driver et al. 2009, , respectively). These surveys provide us with photometry and multi-band imaging of millions of galaxies, and spectroscopy of hundreds of thousands of them. The main results produced by these massive datasets were reviewed by Blanton & Moustakas (2009), describing in detail the physical properties of these galaxies, including their global distributions in luminosity, stellar and atomic gas and their corresponding mass/luminosity functions, for different environments. Despite the huge amount of information and the step forward introduced by these surveys, they had a severe limitation: they do not provide resolved spectroscopic information. Galaxies have long been known to be spatially extended objects, with observed properties that vary across their optical extent (e.g. Hubble 1926, 1936). Many of these properties vary systematically as a function of position relative to the galaxy center, and radial gradients have been studied for decades in both the gas and stellar population content (e.g. Pagel & Edmunds 1981, Peletier 1989). Therefore, to characterize galaxies by single aperture spectra or spatially resolved multi-band photometry imposes severe limitations in both the description of their properties and the understanding of the evolution that shaped them.

This is particularly important in: (i) the study of the variation of the physical properties of the Interstellar Medium (ISM); (ii) the detailed understanding of the composition of the stellar populations across the optical extension of galaxies; and (iii) for the analysis of the kinematic properties and dynamical state of galaxies. To address properly these issues, spatially resolved spectroscopic information is required, covering a substantial fraction of the optical extension of galaxies and for a large, well defined, statistically significant sample, that cover the widest range of galaxy populations in different properties (e.g., masses, colors, morphologies...). The advent of wide-field and multiplexed Integral Field Units (IFUs) in the last decade have allowed us to perform these studies in an efficient way, making it possible to observe large samples of galaxies, and leading to the first generation of Integral Field Spectroscopy (IFS) galaxy surveys (IFS-GS).

Along this review, I will summarize our current knowledge of the spatially resolved spectroscopic properties of low-redshift galaxies based mostly on the results of more recent IFS-GS. I will focus on star-forming galaxies, although I will also present the properties of their retired counter-parts too, as a necessity to discuss our knowledge about what triggers and halts star-formation. This review is therefore focused on the cycle of birth, evolution and death of stars from a statistical point of view. I will summarize the main results on the distributions of stellar populations, properties of the ionized ISM, and their interconnections. First, I will present the main global properties of galaxies, focused on those aspects, to present later the spatial distributions of the same properties. Finally I will present

ISM: Interstellar Medium: gas and dust within a galaxy distributed among and beyond stars.

IFU: Integral Field Unit: a device attached to an spectrograph that allows to obtain several spectra simultaneously of different contiguous locations in the sky.

IFS: Integral Field Spectroscopy: technique that allows to obtain spectra using an IFU.

IFS-GS: Integral Field Spectroscopy Galaxy Survey: Large program to acquire IFS data over a well defined and statistically representative sample of galaxies.

the local scaling laws that we think rule the star-formation and enrichment processes in galaxies. I do not address in this review the morphological and photometric properties of galaxies, or any results that could be derived using only photometric or integrated spectroscopic data (see Blanton & Moustakas 2009, for a review on the topic). The kinematic properties and the dynamical stage of galaxies is not addressed neither (see Cappellari 2016, for a review on the topic). For a more detailed exploration of the emission line properties of galaxies I refer the reader to the recent review by Kewley et al. (2019).

2. DATA

As indicated before, the results shown in this review are extracted from the most recent published analysis on IFS-GS data. Instead of using published figures, along this review I recreate the results based on a compilation of IFS datasets created by combining the data from four different surveys: AMUSING++ (Galbany et al. 2016), CALIFA (Sánchez et al. 2012a), MaNGA (Bundy et al. 2015), and SAMI (Croom et al. 2012). It is beyond the scope of this manuscript to review in detail the different IFS-GS. Nevertheless, I present a summary of their properties in Appendix A, describing the number of galaxies sampled by each survey and the differences in spatial and spectral resolution. Despite the big differences in the nature of these surveys, in particular in terms of the covered area for the sampled galaxies and the spatial and spectral resolution, all of them provide with spatially resolved spectroscopic information for statistical significant and large samples of galaxies mostly located at $z \sim 0.01$-0.06. All together the adopted compilation comprises 8,234 galaxies. That is, so far, the largest compilation of IFS data. A summary of the properties of this compilation is included in Appendix A, and a full description will be given elsewhere (Sánchez et al., in prep.). Along the review I will use this full sample to describe global properties, when required. To present the spatial resolved or radial properties I selected a subset of this sample comprising only those galaxies/datacubes with stellar masses within 10^6 and 10^{13} M$_\odot$, and a redshift range between $0.005 < z < 0.05$, and fulfilling the following criteria: (i) the IFS data cover at least 1.5 R$_e$ of the galaxy; (ii) the galaxy is well resolved, i.e., the effective radius (R$_e$) is larger than 5 arcsec (since most of the IFS-GS have a typical spatial resolution of FWHM$\sim$2.5 arcsec) ; (iii) it is not highly inclined (i.e., ellipticity, ϵ <0.75); (iv) the FoV of the IFS data covers at least 25 arcsec projected in the sky (i.e., sampling at least 2.5 R$_e$). This sub-sample comprises 1,516 galaxies with the best compromise between spatial resolution and sampled IFS data. To homogenize as much as possible the dataset I will make use of the dataproducts provided by the same analysis pipeline, Pipe3D (Sánchez et al. 2016c,b). This pipeline extract the main spectroscopic properties of the galaxies, both integrated, radial and spaxel-wise, including: (i) the composition and kinematic properties of the stellar population, providing with the star-formation and chemical enrichment histories, and main average/integrated properties (stellar mass, age, [Z/H], dust attenuation), together with the velocity and velocity dispersion; (ii) the main properties of a large number of emission lines within the considered wavelength range (flux, velocity, velocity dispersion and equivalent width); (iii) a set of high order physical parameters, like the ISM oxygen abundance derived using different calibrators, the dust attenuation, estimations of molecular gas content, etc. Full details of the delivered products are provided in some recent articles (e.g. Ibarra-Medel et al. 2016, Sánchez et al. 2018, Ibarra-Medel et al. 2019). Pipe3D is just one of the different pipeline/tools developed in the last years with the goal of analysing IFS data (e.g., PyCASSO, LZIFU, MaNGA DAP, de Amorim et al. 2017, Ho et al. 2016, Belfiore et al. 2019b). I adopted it just to homogenize the dataproducts included along this review. In most cases this pipeline produces the same or very similar results to the ones published in the reviewed articles (based in many cases on the tools listed before or similar ones). In case of significant differences or lack of consensus I tried to highlight them as much as possible.

R$_e$: Effective radius: galactocentric distance at which it is encircled half of the total the flux intensity in a certain photometry band of a galaxy.

3. Global properties of Galaxies

As indicated in the introduction, recent reviews have dealt with the description of the current knowledge of the integrated/global properties of galaxies in the near universe, mostly based on single aperture spectroscopic data combined with broad-band imaging photometry (e.g. Blanton & Moustakas 2009). In this section I summarise the main integrated properties and relations that are relevant for the main scope of this review, i.e., the local/resolved properties and relations.

3.1. What ionizes gas in galaxies?

The ISM in galaxies is observed in the optical range mostly by the emission lines produced either by recombination or by radiative desexcitation of collisionally excited levels. To produce emission lines, the gas should be first ionized by high energy photons (of at least 13,6 eV) emitted either by stars (young and old) or active galactic nuclei (e.g. Osterbrock 1989), or generated by the energy dissipation in a shock front travelling through the ISM (e.g. Veilleux & Osterbrock 1987, Veilleux et al. 2005). All the four different sources of ionization may be present in a single galaxy: (i) regions ionized by young OB stars residing in H II regions (Strömgren 1939), associated with star-forming areas (like spiral arms) (e.g. Baldwin et al. 1981); (ii) regions ionized by old stars, post-AGBs or HOLMES (e.g. Binette et al. 1994, Flores-Fajardo et al. 2011), associated with retired regions in galaxies (e.g. Singh et al. 2013, Gomes et al. 2016a); (iii) AGN ionization, mostly concentrated in the central regions (e.g. Husemann et al. 2010, 2014, , although the extension depends on the AGN luminosity); and (iv) shock ionization, either driven by AGN or star-formation outflows (e.g. Heckman et al. 1990, Bland-Hawthorn 1995, López-Cobá et al. 2017b), or driven by low density gas (e.g. Dopita et al. 1996, Kehrig et al. 2012a, Cheung et al. 2016). Since the source of ionization is always local, and not global, to describe the ionized gas of a galaxy by average or integrated properties it is always misleading. A galaxy is neither a star-forming galaxy, a retired galaxy, an AGN or an outflow. A galaxy may present, locally, star-forming and/or post-AGB ionization, and it may host an AGN and enhibits outflows which are able to ionize the gas via shocks. Therefore, the classification for source of ionization in a galaxy should be local, and may require spatially resolved information of the emission line diagnostics. Moreover, as postulated by different authors (e.g. Stasińska et al. 2008, Cid Fernandes et al. 2010, Papaderos et al. 2013, Sánchez et al. 2014, Lacerda et al. 2018), it may require some knowledge of the properties of the underlying stellar population, and even the spatial distribution of the ionized gas structure (e.g. López-Cobá et al. 2019). Based on all those results I present a practical scheme to classify the ionization in Appendix B.
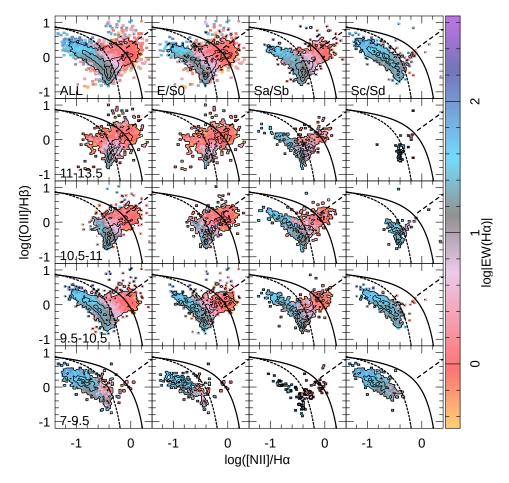
Figure 1 shows the BPT diagram (Baldwin et al. 1981) for the global [O III/Hβ] and [N II]/Hα line ratios, averaged along the entire field-of-view of the IFU data for each galaxy. The plot is color coded by the average EW(Hα) of each galaxy. I present the distribution for the full compilation of galaxies adopted in this review, segregated by both mass and morphology in the different panels. Thus, each galaxy contributes as a single point in each panel, and it is characterized by a single pair of the considered line ratios (e.g. Kauffmann et al. 2003). In addition I include the classical demarcation lines that are usually adopted to classify the main ionizing processes (Kewley et al. 2001, Kauffmann et al. 2003). Line ratios at the left-side of the diagram, with high EW(Hα) are usually associated with ionization by young stars, and therefore related to star-formation processes (H II regions). On the contrary, the right-side of the diagram (above the considered demarcation lines), is associated with hard ionization that could be due to AGNs or shocks (high EWs), or ionization by old stars (e.g., post-AGBs, with low EWs).

Although it is clear that ionization has a local nature, there are clear trends between the global properties of galaxies (e.g., stellar mass, morphology...) and the dominant ionizing source (e.g. Kauff-

post-AGB: Final evolution period of low- and intermediate-mass stars is a rapid transition from the Asymptotic Giant Branch towards the white dwarf phase.

HOLMES: Hot low-mass evolved stars, mostly in the post-AGB or white dwarf phase.
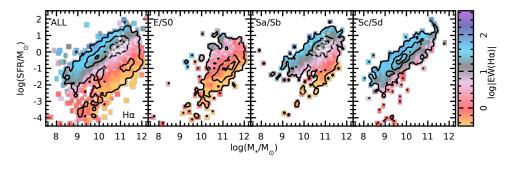
Figure 1

Distribution along the classical [O III/Hβ] vs. [N II]/Hα diagnostic diagram, where each of the 8,234 galaxies included in the adopted compilation contributes as a single point. Color coded is indicated the average equivalent with of Hα across the field-of-view of each datacube. Contours represent the density of galaxies, with each contour including a 95%, 50% and 10% of the points. In all panels, the solid-line represents the location of the Kewley et al. (2001) boundary line, with the separation between Seyferts and LINERs is indicated with a dashed-line. Finally, in the dotted line represents the location of the Kauffmann et al. (2003) demarcation line. Each panel represents a sub-sample of galaxies: the full sample is shown in the upper-left panel, and each panel shows a sub-sample of galaxies segregated by morphology (from left to right) and stellar mass (from top to bottom), with the covered ranges labeled in top- and left-most panels.

mann et al. 2003). This is clearly appreciated in Fig. 1: more massive/early-type galaxies show a stronger contribution of ionization due to old stars, while less massive/later-type galaxies have a stronger presence of ionization due to young stars. This reflects the known evolution of galaxies, since more massive/early-type galaxies formed stars earlier in the cosmological time (e.g. Pérez-González et al. 2008, Thomas et al. 2010, González Delgado et al. 2014b), and therefore they have a larger fraction of old stars (e.g. González Delgado et al. 2016). Finally, AGNs are more frequently found in massive galaxies, either early-type (e.g. Kauffmann et al. 2003) or early spirals (e.g. Schawinski et al.

2010, Sánchez et al. 2018). A more detailed discussion on the ionization processes in galaxies and the use of emission lines to explore their evolution was recently presented by Kewley et al. (2019).

3.2. SFR-M∗ diagram and the SF-law

SFR-M∗ diagram for all the galaxies included in the IFS compilation presented along this review (left panel), and in different sub-groups segregated by morphology, from more early-types to more late-types, from left to right. All panels represent the distribution adopting the SFR estimated based on the dust corrected integrated the Hα luminosity following Sánchez et al. (2018). In each panel, the contours corresponds to the density of points, with each contour including a 95%, 50% and 10% of the points. In all panels, the logarithm of the equivalent with of Hα is color coded, following the same code previously shown in Fig. 1. Finally, the white circles in each panel, show the location of the optically selected AGNs (as selected in Sánchez et al. 2018, too).

Star-forming galaxies (SFGs) are those in which the main ionizing source is the vast presence of OB-stars, directly connected with recent star-formation due to their short life-time (e.g., Pozzetti et al. 2010). On the contrary, retired galaxies (RGs) are those with a lack of ionized gas or with gas ionized by old stars, in which there is little (e.g. Gomes et al. 2016b) or no star-formation (e.g. Stasińska et al. 2008, Cid Fernandes et al. 2010). In general, there are no galaxy (or very few) where the ionization is dominated by shocks induced by outflows. An interesting counter example is the case the filamentary or biconical ionized gas detected in weak AGNs and radio-galaxies (already observed using narrow band images in cD galaxies decades ago, e.g. M87, Jarvis 1990). Kehrig et al. (2012a), using CALIFA data, first proposed that the ionization in these structures (and indeed across all the optical extension of these galaxies) is dominated by shocks. Cheung et al. (2016) proposed them as a new type of objects (named Red Geysers), and their connection with radio-sources was revisited recently by Roy et al. (2018). However, those galaxies comprises less than a 4% of the total elliptical ones (i.e., less than 1% of the total galaxy population), as shown by Lopez-Coba et al. in prep.

On the other hand, AGN ionization may dominate the integrated properties of the emission lines in galaxies, in particular at the central regions. Thus, some galaxies are classified as AGNs, although AGN hosts is a better term (e.g. Kauffmann et al. 2003). When the SFR derived using the dust-corrected Hα luminosity of a galaxy (or any other SFR estimator like UV or FIR luminosities, e.g., Catalán-Torrecilla et al. 2015) is plotted along the stellar mass (M∗), the two populations of SFGs and RGs are clearly distinguished (and indeed well separated by the average value of the EW(Hα), with 3-6 Å being a clear boundary, e.g. Stasińska et al. 2008). This is clearly appreciated in Figure 2, where I present the SFR-M∗ diagram for the galaxies in the current compilation.
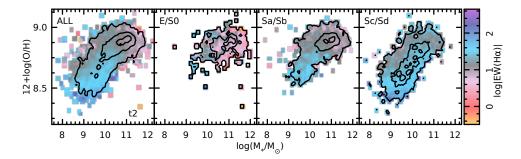
The distribution of SFGs is well characterized by a log-linear, tight relation, observed between the SFR and M∗. This relation, known as the star-formation main sequence (SFMS) of galaxies has been well studied using both single-aperture and IFS data at low-redshift (e.g. Brinchmann et al. 2004,

Daddi et al. 2007, Elbaz et al. 2007, Noeske et al. 2007, Gavazzi et al. 2015, Renzini & Peng 2015, Catalán-Torrecilla et al. 2015, Cano-Díaz et al. 2016, Sánchez et al. 2018). In general, it has a scatter of ~0.2-0.3 dex in SFR at any redshift, with a slope slightly smaller than one at low-redshift, ~0.8 dex/log(M_*). It presents a clear evolution in the zero-point that increases with redshift (e.g. Speagle et al. 2014, Rodríguez-Puebla et al. 2016). On the other hand, RGs are distributed well below the SFMS, following either a loose relation with the M_* (or a cloud), broadly corresponding to the location expected for an EW(Hα)~1Å (e.g. Stasińska et al. 2008). In between the two groups there is an area with much lower number density of galaxies, known as the green valley (GV). Galaxies in the GV (or GVGs) are considered in transit between SFGs and RGs, and their limited number has been interpreted as a consequence of a fast process transforming the former to the later ones (e.g., Bell et al. 2004, Faber et al. 2007, Schiminovich et al. 2007). More recently, it was found that AGN hosts are also located in the GV of the SFR-M_* diagram (e.g. Torres-Papaqui et al. 2012, Schawinski et al. 2014, Cano-Díaz et al. 2016, Sánchez et al. 2018), as appreciated in Fig. 2. Actually, their distribution is spread from the SFMS towards the RGs cloud, covering mostly the GV, and sharing many properties with GVGs (e.g. Sánchez et al. 2018). This result suggests that there is a connection (or co-evolution) between the AGN activity and the quenching of star-formation in galaxies.

The key ingredient of star-formation is cold gas, from which stars are formed (see e.g., Kennicutt & Evans 2012, Krumholz et al. 2012). Indeed, Schmidt (1959) already suggested a relation between the SFR and the interstellar gas volume density. This relation was later observed as a relation between the surface densities of both quantities, and it is known as the Schmidt-Kennicutt or star-formation law (Kennicutt 1998a). This relation is maintained at kpc-scales only for the molecular gas (e.g., Kennicutt et al. 2007, Bigiel et al. 2008, Leroy et al. 2013, and references therein). It is beyond the scope of this review to explore in detail the global star-formation law and the detailed connection of cold gas with the star-formation process. However, for the sake of understanding the local processes described later, I should indicate that RGs present a clear deficit of both atomic and molecular gas (e.g. Saintonge et al. 2016, Calette et al. 2018). Thus, the lack of cold gas seems to be the primary reason for the limited SFR (if any). How this deficit of gas is connected to the presence of an AGN is a topic of study, being both heating and removal the main explanations invoked through the so-called negative feedback (e.g. Silk 1997). Indeed, there are other possible sources of low gas content, related with gas interactions, harassment and stripping, more related with externals processes (e.g. Poggianti et al. 2017).

However, even for the same amount of cold gas, galaxies may present a different star-formation efficiency, SFE=SFR/M_{gas}, (e.g. Saintonge et al. 2011) or different scaling factors between the two parameters involved in the star-formation law (e.g. Elmegreen et al. 2007). Indeed, Colombo et al. (2018) show that the SF is less efficient in more early-type galaxies beside the fact that they have less amount of molecular gas. In summary, the lack of gas is the primary driver for the halting of SF, but a secondary cause involves a decline in the SFE.

3.3. Gas phase Mass-Metallicity relation

Metals are produced as a result of the thermonuclear reactions that make the stars shine, and during their super-novae explosion phase (when it happens). After their death (and along their life-time too, e.g. Yates et al. 2012), metals are expelled to the ISM, polluting it, and enriching the next generations of stars. Therefore, the metal content in the ISM is a tracer of the previous generations of stars, modulated by the gas inflow, outflow and depletion processes. Among the different metals, oxygen is particularly interesting, being the most abundant one (and the most frequent element after H and He, e.g., Peimbert et al. 2007). Being an α-element, it is expelled mostly by core-collapsed supernovae generated by the death of short-lived massive stars, and therefore its relative enrichment is tightly related to last star-

Figure 3

Gas-phase mass-metallicity relation for the collection of IFS observed galaxies adopted along this review with abundances measured at the effective radius (~4600 galaxies). All panels correspond to the MZR derived using the *t*2 calibrator (defined in Sánchez et al. 2019b). The left-most panels show the distribution for all the galaxies, with similar distributions segregated by morphology shown in the different panels, from earlier types to later ones from left to right. Like in Fig. 2, the distributions are shown as density contours, with each contour including a 95%, 50% and 10% of the points. Finally, the color indicates the mean value of the EW(Hα) for all galaxies contributing to each point in the distribution, following the same code previously shown in Fig. 1.

formation events. As a consequence it is both a tracer of the overall chemical evolution of galaxies, being a by-product of SF, and a local proxy of the differential SF activity.

Averaged across the optical extension of a galaxy, the oxygen abundance correlates with the integrated stellar mass. This relation, known as the MZ-relation or MZR (although a more correct name should be the M_*-O/H relation), connects the two main products of star-formation integrated along the cosmic time. Known for decades (e.g. Vila-Costas & Edmunds 1992), it was originally expressed also as a luminosity-O/H relation (e.g. Garnett 2002). Tremonti et al. (2004) made the first systematic exploration of this relation using a statistically large and significant sample of galaxies, showing that the two parameters exhibit a tight relation, with a dispersion lower than ~0.1 dex, covering more than four orders of magnitude in M_*. More recent analysis reduces this scatter to ~0.05 dex (e.g. Sánchez et al. 2018). Figure 3 shows the distribution along the M_*-O/H diagram for the full sample of galaxies adopted along this review, using a particular calibrator. The shape of the MZR is clearly appreciated. A full exploration of the differences reported when using different calibrators was already discussed by Kewley & Ellison (2008), and more recently revisited by Barrera-Ballesteros et al. (2017), Sánchez et al. (2017) and Sánchez et al. (2019b). The MZR presents an almost linear regime for $M_* < 10^{10} M_\odot$, flattening between 10^{10}-$10^{10.5} M_\odot$, and reaching a plateau for more massive galaxies. The extension of the linear regime, i.e., the location of the M_* knee, and the actual asymptotic value depends on the adopted calibrator or procedure used to measure the oxygen abundance (e.g. Barrera-Ballesteros et al. 2017), and the Initial Mass Function (IMF Salpeter 1955) adopted in the derivation of the M_*. However, the shape is almost universal both in the nearby universe (e.g. Kewley & Ellison 2008, Sánchez et al. 2017, 2019b), and at different redshifts (e.g. Erb et al. 2006, Erb 2008, Henry et al. 2013, Salim et al. 2015).

At low stellar masses the linear relation between the two parameters is interpreted as a direct consequence of the star-formation history (SFH) in galaxies, dominated at this regime by a consistent growth of both parameters as integrals of the SFR (modulated by the effective yield in the case of O/H). This regime of the relation indicates that the evolution does not depart too much from the one predicted by a close-box model (e.g. Pilyugin et al. 2007). The larger differences from a close-box model are found in the asymptotic regime, in which an increase in the stellar mass does not produce a

significant increase in the oxygen abundance. Tremonti et al. (2004) already interpreted this flattening as a result of galactic outflows that regulate the oxygen abundance (by removing metal rich gas from galaxies). Different studies support this interpretation (e.g. Davé et al. 2011, Lilly et al. 2013, Belfiore et al. 2016, Weinberg et al. 2017). An alternative interpretation is that gas inflow can produce a similar shape for the MZR, with the asymptotic value being a natural consequence of the maximum amount of oxygen that can be produced by stars, i.e., the yield. Pilyugin et al. (2007) already showed that the observed asymptotic value is compatible with the yield predicted by a closed-box model for a gas fraction f_{gas} ~5-10%, assuming a value of the oxygen abundance derived using calibrators anchored to the direct method. However, recent studies indicate that gas outflows are still required to reproduce the observed shape (e.g. Barrera-Ballesteros et al. 2018).

More controversial is the presence of a secondary relation between the MZR and the SFR (once removed the primary relation between O/H and M_*). Ellison et al. (2008) first reported the existence of this secondary relation, that latter on has been proposed as (i) a modification of the stellar mass by a parameter that includes both this mass and the SFR (e.g. Mannucci et al. 2010, known as the Fundamental Mass-Metallicity relation or FMR), (ii) as a fundamental plane involving the three parameters (e.g. Lara-López et al. 2010, known as the Mass-Metallicity-SFR Fundamental Plane), or (iii) as a dependence of the residuals of the primarly relation with the SFR or the sSFR (e.g. Salim et al. 2014). In most of the cases it is described as a trend in which galaxies with larger SFR at a fixed mass present a lower metallicity. Both galaxy inflows and outflows have been proposed to explain the secondary relation (e.g. Sánchez Almeida & Sánchez-Menguiano 2019). The existence of this secondary relation has been questioned by studies based on IFS data (e.g. Sánchez et al. 2013, 2018, Barrera-Ballesteros et al. 2017, Sánchez et al. 2019b), contrary to most of the previous ones based on single aperture spectroscopic surveys (e.g., SDSS). In some cases, the existence or not of the FMR depends on the interpretation of the data, as shown by the re-analysis of the IFS data presented by Salim et al. (2014) and Cresci et al. (2019). It is beyond the scope of this review to enter in this discussion, that has been addressed in more detail recently by Maiolino & Mannucci (2019).
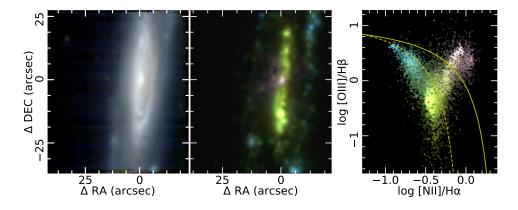
3.4. Age and Metallicity distributions in galaxies

It is known that galaxies present a clear bimodal distribution in many different properties that are likely physically connected. In particular, they present a clear bimodality in the SFR-M_* diagram discussed in Sec. 3.2, which is directly connected with the morphological segregation between early- and late-type galaxies already introduced by Hubble (1926). This bimodality has been more frequently explored using color-magnitude diagrams (CMD, e.g. Strateva et al. 2001, Blanton et al. 2003, Bell et al. 2003), with early-type/RGs located along a well defined region known as the *red-sequence*, and late-type/SFGs distributed in the so called *blue-cloud* (as nicely reviewed by Blanton & Moustakas 2009). A more physically motivated version of the CMD is the Age-M_* diagram, where galaxies clearly show a sharp bimodal distribution (e.g. Gallazzi et al. 2005, 2008, Sánchez et al. 2018). This diagram shows that early-type galaxies (E/S0) are strongly dominated by a very old stellar population of ~10 Gyr, with a narrow distribution of ages. This is a direct consequence of a SFH dominated by a strong burst at early cosmological times (e.g. Panter et al. 2003, Thomas et al. 2005, García-Benito et al. 2017), frequently modelled with a single burst of star-formation. On the contrary, late-type spirals (Sc/Sd) contain a considerable fraction of old stars, of a similar or slightly lower ages, but with a substantial amount of stars younger than 1 Gyr, and a much wider range of stellar ages. Again, this indicates that they present a smoother evolution (e.g. López Fernández et al. 2016, García-Benito et al. 2017, Sánchez et al. 2019a), and a wider variety of SFHs (e.g. Ibarra-Medel et al. 2016). As expected, early-type spirals (Sa/Sb) present a mixed behavior. Their older populations have similar ages to those

of the early-type galaxies. However, the contain a considerable fraction of young stellar populations too, with ages similar to those of the late-type spirals.

Contrary to the global stellar ages, stellar metallicity ($[Z/H]_*$) does not show any clear evidence of a bimodal distribution, showing a smooth relation with M_* (e.g. Gallazzi et al. 2005, Panter et al. 2008, Vale Asari et al. 2009, González Delgado et al. 2014a, Sánchez et al. 2018). Stellar metallicity is a by-product of the star-formation process. However, contrary to the gas phase abundance, which increases with each generation of new massive stars formed (and death), modulated by inflows and outflows, stellar metallicity traces the metal content in the surviving stars (i.e., those of intermediate and low mass). Therefore, its interpretation and the relation with the stellar mass is less evident than that of the oxygen abundance. On the other hand, the derivation of the stellar metallicity depends strongly on data used (photometry/spectroscopy, wavelength range...) and the method adopted to explore the stellar populations: full fossil records, SFHs and Chemical Enrichment Histories (ChEHs) adopted or not, comparison with single stellar populations, inclusion or not of the $[\alpha/Fe]$ relative abundances (e.g. Walcher et al. 2011, Conroy 2013). Despite these caveats the lack of bimodality indicates that the quenching process does not affect the metal enrichment significantly, that, in any case, is frozen to the last episode of SF.

4. Resolved properties of Galaxies

Along the previous sections I have summarized the main properties of galaxies derived from integrated or aperture limited spectroscopic surveys. In the current section I will review how these properties are extended to local scales (i.e., ~1 kpc), as uncovered by more recent IFS Galaxy Surveys.
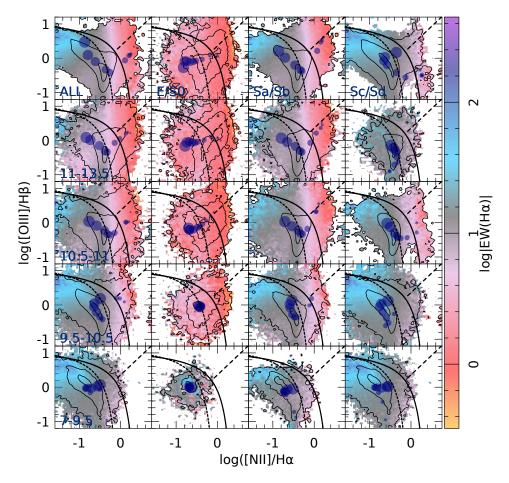

Figure 4

Each panel shows, for galaxy IC1657 observed with MUSE (PI:R.Bacon): (i) the continuum image created using g (blue),r (green) and i-band (red) images extracted from a MUSE datacube, by convolving the the individual spectra with each filter response (left-panel), (ii) the emission line image created using the [O III] (blue), Hα (green) and [N II] (red) emission line maps extracted from the same datacube using the Pipe3D pipeline (central-panel), and (iii) the classical BPT diagnostic diagram involving the [O III]/Hβ and [N II]/Hα line ratios. Each point in this diagram corresponds to a single pixel (spaxel) in the other two maps, represented with the same color shown in the emission-line image (central panel). The solid- and dashed-lines represent the location of the Kewley et al. (2001) and Kauffmann et al. (2003) demarcation lines, respectively. *(credits. C. López-Cobá)*

Ionization is a local process: all sources of ionizing photons are local, not global. A galaxy does not have a single source of ionization.

Classical [O III/Hβ] vs. [N II]/Hα diagnostic diagram for the spatially resolved distribution of the ionized gas across the optical extension of the considered sample of galaxies. Color coded is the average of the logarithm of the equivalent with of Hα at each location, and contours represent the density of spaxels, with each contour including a 90%, 50% and 10% of the points. Blue solid-circles represent the baricenter of the density distribution at different galactocentric distances, represented by the size of circles, ranging from 0.1 R_e (smallest circle) to 2.1 R_e (largest circle). In all panels, the solid-line represents the location of the Kewley et al. (2001) boundary lines, with the separation between Seyferts and LINERs indicated with a dashed-line. Finally, in the dotted-line represents the location of the Kauffmann et al. (2003) demarcation line. Each panel represents a sub-sample of galaxies: the full sample is shown in the upper-left panel, and each panel shows a sub-sample of galaxies segregated by morphology (from left to right) and stellar mass (from top to bottom), with the covered ranges labeled in top- and left-most panels.

4.1. Ionized gas across the optical extension of galaxies

As indicated in Sec. 3.1 the ionization in galaxies is produced by local processes, that may be different in different locations within each galaxy. Averaged across this extension, the properties of the ionized gas reveal either the dominant physical process or a mixture of all of them (e.g. Kauffmann et al.

2003). This is illustrated in Figure 4 where two composite images are shown, one constructed based on the *g* (blue), *r* (green) and *i*-band (red) continuum images and the other one based on the [O III] (blue), Hα (green) and [N II] (red) emission line maps, extracted from the MUSE observations of the galaxy IC1657 corresponding to the AMUSING project (PI: J. Anderson, e.g. Sánchez-Menguiano et al. 2018). The right-most panel shows the classical BPT diagnostic diagram (already discussed in Sec. 3.1 and shown in Fig. 1). In this case each dot in the BPT diagram corresponds to a pixel in the RGB emission-line image, and it is represented by the same color shown in that image (central panel). This allows us to easily identify the location within a galaxy at which different ionization happens. A clear bi-conical ionized gas structure is seen in the center of this galaxy, highlighted as pink colors, indicating strong [N II]/Hα and [O III]/Hβ line ratios (as seen in the BPT diagram). This structure is a clear signature of shock ionization induced most probably by an outflow driven by a strong nuclear star-formation event (e.g. López-Cobá et al. 2017b, 2019, López-Coba et al., in prep.). In addition to this structure, it is easy to identify, in the emission-line image, the star-forming regions across the inclined disk, with a clear gradient in the line ratios, which are recovered by the green colours towards the center, and bluish colors in the outer part. This change in the line ratios is frequently interpreted as a signature of the oxygen abundance gradient observed in disk galaxies (e.g. Searle 1971, Vila-Costas & Edmunds 1992, Sánchez et al. 2014). This object is used to illustrate that different ionization sources could be present at different locations within each galaxy. In general all sources of ionization described in Sec. 3.1 maybe be present simultaneously (or not) in different galaxies.

Despite the different ionization sources that may be present in a single galaxy, there are patterns within galaxy types, similar to those described for the integrated/average properties. Figure 5 shows the distribution of individual ionized regions in a subset of the galaxy sample explored in this review within the classical BPT diagnostic diagram (i.e., the same adopted in Fig. 1, for integrated quantities). The position of individual regions depends on the mass and morphology of the host galaxy; regions belonging to more massive and early type galaxies populate the right-hand side of the diagram, with lower values for the EW(Hα). On the other hand, for late and less massive galaxies more ionized regions populate the left-hand side of the diagram with larger values of the EW(Hα). However, contrary to what is seen for the integrated properties of galaxies (shown in Fig. 1), for the spatially resolved regions a wider range of parameters is covered in most of the diagrams. This reflects the fact that the average properties do not represent the full range of ionization conditions found across the optical extension of individual galaxies (as shown in Fig. 4).

The distribution of ionized regions does not depend only on the properties of the hosting galaxy, but also on the location within the galaxy. The baricenter of the density distributions along the diagram for different galactocentric distances in included in Fig. 5 as blue solid-circles. For doing so I estimate the same density distribution shown as contours, but in consecutive radial bins centred at consecutive galactocentric distances between 0.1R$_e$ and 2.1R$_e$, and a width of 0.2R$_e$ (following the position angle and ellipticity of each individual galaxy). The size of the circles increases with the galactocentric distance of the considered ring. For most galaxy types and stellar masses there is a clear trend with the radial distance. The ionized regions in the center of galaxies (R<R$_e$) are mostly located in the upper-right of the diagram. On the other hand, the outer regions are located either at the upper-left (or left) (for most of late-type galaxies, apart from the lowest mass ones) or at the bottom-left (for early-type ones). However, there are substantial differences for different galaxy types and stellar masses. Early-type galaxies lack the left-side branch corresponding to SF regions in general, and the trend goes just from the upper-right to the bottom-center. Finally, as lower is the mass, as narrower seems to be the covered range of parameters, in particular for the [N II]/Hα ratio, and the trend is even reverse for Sc/Sd galaxies.

The explanation for these distributions has been discussed in different articles. For the center of
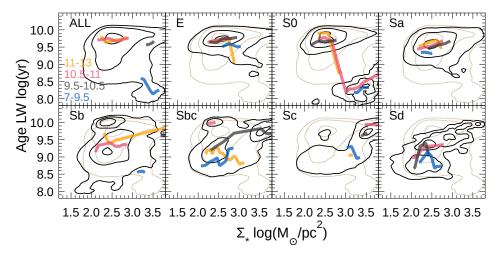
most massive and early type galaxies, the location in the diagram and the low observed values for the EW(Hα) indicate that the dominant ionization is due to ionizing old stars, post-AGBs or hot low-mass evolved stars (HOLMES Binette et al. 1994, Stasińska et al. 2008, Cid Fernandes et al. 2010). Recent results have shown that this ionization, observed as a diffuse extended ionization in the central regions of early-type galaxies by Sarzi et al. (2010) and Gomes et al. (2016b), is ubiquitous in galaxies of different morphology at the location of old-stellar populations (Singh et al. 2013, Papaderos et al. 2013, Sánchez et al. 2014). This result was recently confirmed by Belfiore et al. (2017c) and Lacerda et al. (2018). The observed trend from the upper-right towards the lower left of the diagram from the center to the outer regions could be explained by a change in the average age of the ionizing population, in agreement with the predictions by models (e.g. Morisset et al. 2016). This result highlights the connection between the observed properties of the ionized gas and those of the stellar populations, showing that in early-type galaxies there should be a negative gradient in the average age of the stellar population, as indeed it is observed (e.g. González Delgado et al. 2014b). Finally, for a few early-type galaxies, in particular the less massive ones, there is some marginal star-formation activity, as shown by Gomes et al. (2016b). This star-formation could be a residue of a former activity that declines due to the natural dimming or ageing of the disk (e.g. Casado et al. 2015), or a rejuvenation due to the capture of pristine gas or a gas-poor low-mass galaxy by the early-type one (e.g. **?**).

The connection with the properties of the stellar populations is even more clear for the late-type galaxies. In those galaxies there is some ionization due to old stars in the central regions for early-type spirals, i.e., spirals with bulge (Sa/Sb) at R<R$_e$. This is more clearly appreciated in the average distribution of these galaxies and for most massive ones (upper panels of third column in Fig. 5). For the later-type spirals (Sc/Sd), galaxies without a prominent bulge, the location of the central ionized regions in the diagram is not well defined. This is in agreement with the results by Singh et al. (2013), as indicated before, since bulges are dominated by older stellar populations. However, the dominant ionization in these galaxies is star-formation, and indeed the corresponding line ratios are found in the regions usually associated with this ionization, i.e., below the Kewley et al. (2001) curve with large values of the EW(Hα). This is where most of the ionized regions are found, in particular for galactocentric distances larger than 0.5 R$_e$. In these galaxies, and in particular in those with a stellar mass larger than $10^{9.5}$M$_\odot$, there is a trend from the bottom-middle towards the upper-left area of the diagram as we move further away in the disk (from 0.5 to 1.5 R$_e$). This trend can be easily explained as a consequence of the well known negative gradient in the gas-phase metallicity in spiral galaxies, that has been found to be very similar for all galaxies in this mass regime (Sánchez et al. 2014, Sánchez-Menguiano et al. 2016b). For the less massive late-type galaxies ($<10^{9.5}$M$_\odot$), there is a less clear or inverted trend, reflecting that in this regime the abundance gradient is less prominent, flat, or even inverted (Belfiore et al. 2017c, Sánchez & Sánchez-Menguiano 2017). In summary, the observed distribution reflects the connection between the ionization conditions in star-forming regions and the overall evolution of the underlying stellar population (as described by Sánchez et al. 2015b). As a consequence of this connection, the location of an H ii region in a diagnostic diagram is mostly determined by the stellar-mass and morphology of its host galaxy and its galactocentric distance. Indeed, this is the reason why we can use H ii regions to trace the chemical evolution of spiral galaxies, including our own galaxy (e.g. Mollá & Díaz 2005, Sánchez-Menguiano et al. 2018, Esteban & García-Rojas 2018, Carigi et al. 2019).

These results show that the ionization through the full optical extension of the general population of galaxies is dominated by stellar processes (either young or old). However, in some particular galaxies (e.g., AGNs, galactic outflows hosts, mergers), there are other ionization processes that can clearly over-shine the effect of these stellar ionizing sources. This is particularly true for certain regions within galaxies (i.e., central regions), but it is also evident when the average/integrated ionization properties are explored (as appreciated in Fig. 1 where AGNs are identified as blue points above the Kewley

curve). However, the frequency of those processes is so low (at least in the nearby universe) and in some cases the spatial extension is so confined to certain regions in galaxies, that they have little influence in the average spatial distributions shown in Fig. 5. In other words, they are blurred by the overwhelming and ubiquitous presence of stellar ionization processes.

4.2. Local Age bimodality: Σ_*-age bimodality

Figure 6

Distribution of the luminosity-weighted ages of the stellar populations along the stellar mass surface densities shown as density contours (encircling 85%, 50% and 15% of the regions), in solid-black lines. Each panel shows the distribution for all galaxies (top-left), and segregated by morphology (from earlier galaxies to later ones, from top-left to bottom-right). In addition, it is shown the trace of peak densities for different stellar mass bins as color solid-lines, with each color representing a M_* bin as indicated in the label (only densities above a 50% are considered in this derivation). Finally, the light-brown solid contours in the panels for each different morphology reproduce the distribution of the full population (shown in the top-left panel)
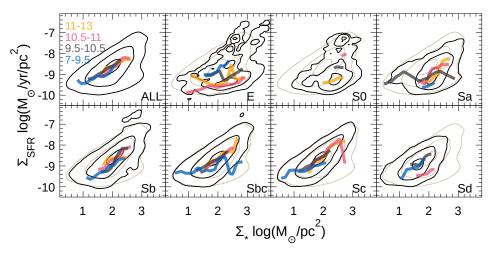
    I show in Section 3.4 that galaxies present a clear bimodal distribution along the M_*-Age diagram. As indicated in that section this diagram is a more physical-driven version of the color-magnitude diagram, used for decades in astronomy to select star-forming and non-starforming galaxies (e.g. McIntosh et al. 2014). González Delgado et al. (2014b) first showed the distribution along the Σ_*-Age diagram for spatially resolved kiloparsec-scale regions of different galaxies, describing a clear trend towards older populations being located in denser regions of more massive galaxies (and in the central regions). More recently, Zibetti et al. (2017) demonstrated that this distribution is bi-modal: the distribution of individual regions within galaxies in the Σ_*-Age diagram present two clear density peaks clustered around old (~9 Gyr) and young (~1-4 Gyr) ages, respectively, mostly related with retired regions (dominant in early-type galaxies), and star-forming regions (more frequent in late-type galaxies). In late-type galaxies (in particular in early-spirals) the central regions, associated with bulges, are found around the old-age peak, while their disks and spirals arms are located around the young-age one. This is a clear indication of an internal/local age bimodality. This result is found as a statistical effect when exploring the full sample, and also in individual galaxies.

    Figure 6 reproduces the results by Zibetti et al. (2017), showing the distribution of individual spaxels in the Σ_*-Age diagram for the compilation explored in this review. I show the distribution

Local bimodality: areas within galaxies present a local bimodality in they Σ_*-age distribution.

for all galaxy types (top-left) and segregated by morphology from earlier to later types (from top-left to bottom-right). In addition, I show the density peak along Σ_* for different stellar masses (colored solid-lines). The bimodality uncovered by Zibetti et al. (2017) is clearly seen, showing a strong morphological dependence (with younger regions located in later type galaxies), and a trend with the stellar masses (with younger regions located in less massive galaxies). Intermediate spirals (Sb/Sbc) show a clear bimodal distribution, highlighting the connection between the two populations with the bulge (old) and the disk (young). Like in the case of the M_*-Age (and CM-diagram), the regions with old stellar populations follow a well-defined region, called old-sequence (resembling the red-sequence in a CM-diagram), with very similar ages (~6 Gyrs) for a wide range of Σ_* values. On the other hand, young stellar populations cover a considerable range of values, from a few hundred of Myrs to a few Gyrs within the same Σ_* range. The bimodality implies an abrupt/short-lived transition, leading to a local quenching of the star-formation or sharp change in the SFHs from the inside-out (e.g. López Fernández et al. 2018, Belfiore et al. 2017b). Moreover, this distribution indicates that all regions with old-stellar population have very similar SFHs (due to the limited range in ages). However, regions with young stellar populations may present a large variety of SFHs (due to the spread of ages). This was indeed described in Ibarra-Medel et al. (2016) and García-Benito et al. (2019).

4.3. Local SFMS: $\Sigma_* - \Sigma_{SFR}$.

Figure 7

Distribution of the star-formation rate surface densities along the stellar mass surface densities shown as density contours following the nomenclature of Fig. 6

I have shown in Sec. 3.2 that galaxies also present a bimodal distribution in the SFR-M_* diagram, with SFGs following a tight correlation (the SFMS) between the two parameters (σ ~0.2-0.3 dex, once removed the main trend). In 2013 two almost simultaneous studies, Sánchez et al. (2013) and Wuyts et al. (2013), analysing completely different samples (at z ~0 and z ~1, respectively) and using different techniques (IFS and narrow-band HST imaging), showed that star-forming regions present a very similar relation between the SFR surface density (Σ_{SFR}) and stellar mass surface density (Σ_*), a relation that holds at kilo-parsec scales. This relation is now known as the resolved SFMS (or rSFMS), and has been confirmed by many different authors using mostly IFS-GS mainly for galaxies in the
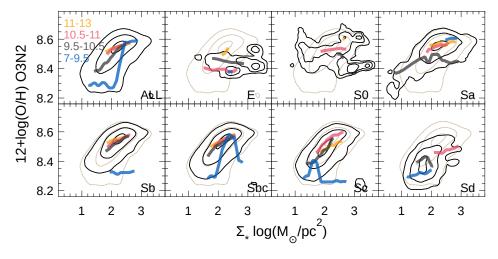
nearby universe (e.g. Cano-Díaz et al. 2016, González Delgado et al. 2016, Maragkoudakis et al. 2016, Abdurro'uf & Akiyama 2017, Hsieh et al. 2017, Pan et al. 2018, Ellison et al. 2018, Medling et al. 2018, Erroz-Ferrer et al. 2019, Cano-Díaz et al. 2019). They all found that this relation is as tight as the global one, with a dispersion between ∼0.2-0.3 dex (once removed the main trend), and a slope slightly below one. To our knowledge there is no formal published comparison between the high-z rSFMS and the low-z ones. However, comparing the best fitted values reported by Wuyts et al. (2013) adopting a log-linear relation with those reported by the most recent analyses at low-z, it seems that the rSFMS relation present a weak evolution in the slope (from $\alpha_{z\sim1}$ ∼0.95 to $\alpha_{z\sim0}$ ∼0.78-0.94, respectively) and a very strong evolution in the zero-point (from $\Sigma_{SFR,2\ z\sim1}=10^{-6.8}$ $M_\odot yr^{-1}pc^{-2}$ to $\Sigma_{SFR,2\ z\sim0}=10^{-8.5}$ $M_\odot yr^{-1}pc^{-2}$, with $\Sigma_{SFR,2}$ being the SFR surface density at $\Sigma_*=10^2$ $M_\odot pc^{-2}$). This evolution is similar to the one reported by the global SFMS (e.g. Speagle et al. 2014, Rodríguez-Puebla et al. 2016), and it is broadly reproduced by the most recent analysis of hydrodynamical/cosmological simulations (e.g. Trayford & Schaye 2019).

Figure 7 shows the distribution along the Σ_{SFR}-Σ_* diagram for the individual spaxels in my compilation, segregated by both morphology and mass. In this particular case I adopted the Σ_{SFR} derived from the Hα emission irrespectively of the ionizing source, following Cano-Díaz et al. (2016), Sánchez et al. (2018) and Cano-Díaz et al. (2019). This way Hα traces either the SFR for star-forming areas (SFAs) in each galaxy, or just an upper-limit to the SFR for non star-forming/retired areas (RAs). The most recent results show that there is a bimodality in the distribution of areas in this diagram (e.g. Hsieh et al. 2017, Cano-Díaz et al. 2019), with SFAs tracing the described rSFMS relation and RAs located in a cloud well below that relation. Depending on the S/N cut applied to the Hα detection (or any other tracer of the SFR), this second cloud is more or less evident. In our particular compilation this cloud is clearly seen only for earlier type galaxies (E, S0 and less clear for Sa), and only as a bump in the distribution for all galaxy types. As reported by the same authors, the RAs cloud is dominated by regions in early-type galaxies, while the rSFMS is dominated by regions in late-type ones, with a clear morphological evolution (as found by González Delgado et al. 2016). For the bulk population of galaxies, irrespectively of their morphology, the density peak in the diagram traces the rSFMS at any mass. Thus, the mass dependence is weaker than the morphological one. Like in the case of the Σ_*-Age bimodality, this is a consequence of the local evolution, with SFAs associated with regions in the disk and RAs associated with regions in the bulge (dominated by quenched regions).

It is worth noticing that the applied cuts in the S/N and the detection limits for properties involved in resolved relations have to be treated with care. Cano-Díaz et al. (2019) explored the effects of detection limits in the shape of the rSFMS and in the artificial generation of broken distributions resembling two-linear regimes (e.g. Erroz-Ferrer et al. 2019).

Besides the increase of the fraction of RAs, some authors (e.g. González Delgado et al. 2016, Cano-Díaz et al. 2019), reported a change in the rSFMS itself with the morphology of the host galaxy. Later-spirals (Sc/Sd) present slightly larger Σ_{SFR} than earlier-spirals (Sa/Sb) for a fixed stellar mass. This is somehow appreciated in Fig. 7, with the rSFMS of Sa (Sc) galaxies being slightly below (above) that of the full population. This result may indicate that the SFH of SFAs in earlier-spirals present a sharper decline with the cosmological time (shorter times scales) than in later-ones, having a lower Σ_{SFR} at $z\sim0$ than in the past. Thus, they present a faster evolution or ageing that the SFAs of purely disk-dominated galaxies. More recently, Ellison et al. (submitted) has demonstrated that the dispersion across the rSFMS is due to changes in the local star-formation efficiency (SFE). This agrees with the described morphological trend, since the SFE does indeed change with galaxy type both globally and locally (e.g. Colombo et al. 2018). Most probably there are dynamical effects, like the stabilisation induced by the bulge proposed by Martig et al. (2009), that precludes the star-formation in earlier-spirals. However, the SFE does not explain why a region is retired, that seems to be more directly

connected with a lack of gas (with the conditions required to form stars), and being driven by global properties, in particular by the presence of a massive central black-hole, as demonstrated by Bluck et al. (in prep.). In other words, SF is governed by local processes (auto-regulation/local feedback) while quenching is driven by global ones (in agreement with the results presented by González Delgado et al. 2014b)

4.4. Local Mass-Metallicity relations

Figure 8

Distribution of the gas-phase oxygen abundances along the stellar mass surface densities shown as density contours following the nomenclature of Fig.6. The O/H was derived based on the M13 calibrator (Marino et al. 2013)
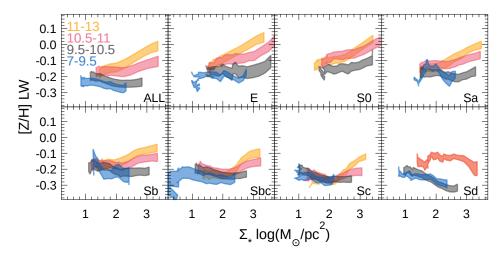
In the previous sections I showed that the stellar populations present a local bimodality in the Age-M_* and SFR-M_* diagrams, with RAs located in a tight *old-sequence* in the first diagram and SFAs following a local rSFMS, in the latter one. These local/resolved counter-parts of global relations and properties have been explored for other parameters, like the MZR. Ryder (1995) already showed that local/spatially-resolved oxygen abundance presents a correlation with the surface-brightness in the optical. This relation suggests the existence of a local/resolved MZR (rMZR hereafter). Like in the case of the rSFMS, this relation was proposed in two independent studies by Moran et al. (2012) and Rosales-Ortega et al. (2012), using different techniques. In the first case classical slit-spectroscopy was used to recover the oxygen abundance along the aperture for a sample of star-forming galaxies in combination with SDSS photometry to estimate Σ_*. The second study explored the relation between oxygen abundance, Σ_* and EW(Hα) for the SFAs (HII regions and clusters) detected using IFS (Rosales-Ortega et al. 2010). Both studies show that there is a relation between Σ_* and O/H with a shape that resembles the global M_*-O/H relation. It presents two regimes, one, just below $\Sigma_* < 10^2$ $M_\odot pc^{-2}$, with an almost log-linear increase of the oxygen abundance with Σ_*, followed by a flattening to an asymptotic value at $\Sigma_* \sim 10^3$ $M_\odot pc^{-2}$. Indeed, Rosales-Ortega et al. (2012) explicitly show that the global MZR relation can be recovered from the rMZR integrating the local one along the optical extension of each galaxy. Subsequent studies confirmed the existence of this local relation using larger samples of galaxies and/or SFAs or IFS data with better spatial resolution (e.g. Sánchez et al.

2013, Barrera-Ballesteros et al. 2016, Erroz-Ferrer et al. 2019). In some cases two-linear relations are proposed for that relation rather than a smooth transition between the two regimes (e.g. Erroz-Ferrer et al. 2019).

Figure 8 shows the distribution in the Σ_*-O/H diagram for the individual spaxels of the explored data-set, once more segregated by morphology and stellar mass. In this particular case only the SFAs have been selected to derive the oxygen abundance, following the criteria outlined in the Appendix B. For the remaining regions the adopted oxygen abundance calibrators may not be valid, as they are anchored to measurements derived for H II regions or photoionization models created to describe these SF ionized structures. Like in the case of the global MZR the shape of the relation is basically preserved irrespectively of the calibrator adopted to estimate the O/H or the assumptions made to derive the stellar mass density. However, the absolute scale of the oxygen abundance changes with the calibrator (in agreement with the expectations of the results found by Kewley & Ellison 2008). Contrary to what it is found for the age bimodality and the rSFMS, the distribution of SFAs in the Σ_*-O/H does not seem to present clear deviations neither with the stellar mass (for $M_* > 10^{9.5} M_\odot$) nor with the morphology (for spiral galaxies) besides the wide range of values covered by each group. In other words, all SFAs seems to be distributed along the same rMZR relation, with more massive galaxies covering the upper-right of the diagram and low-mass (and later-types, e.g., Sd) covering the lower-left range. Clear deviations from this global trend are appreciated for low mass galaxies ($M_* < 10^{9.5} M_\odot$), and maybe the few star-forming regions in elliptical galaxies (E and S0). In the first case the statistic is poor (low number of galaxies). However the result could be interpreted as a consequence of an outside-in chemical enrichment, that I will discuss in the upcoming sessions. On the other hand, for the ellipticals and S0, maybe the few galaxies with detected star-formation (Gomes et al. 2016b) are the consequence of the capture of metal-poor galaxies, rather than an effect of disk dimming. Indeed, in the case of S0 the distribution shows two peaks, one following the main rMZR trend, and another one more similar to the distribution appreciated for pure ellipticals. Unfortunately, even for the large compilation included in here the statistic is too low for SFAs in early-type galaxies.

Recent studies have explored whether the rMZR presents a possible secondary relation with the SFR (Σ_{SFR}), following the concept of the FMR. This secondary relation is commonly interpreted as the consequence of gas inflows and outflows (as discussed in Sec. 3.3). The results of these explorations are not fully conclusive. Some authors claim that there is no secondary relation (e.g. Barrera-Ballesteros et al. 2016, 2017), based on the analysis of the possible dependence of the residuals of the rMZR with the sSFR and Σ_{SFR}. Other authors claim that there are secondary trends between the residuals of the radial distributions of the Σ_{SFR} and O/H (e.g. Sánchez-Menguiano et al. 2019), that at low-mass are negative and at high-mass positive. This may be interpreted as evidence for a local/resolved FMR (or rFMR, Sánchez Almeida & Sánchez-Menguiano 2019). However, radial migration and the local effect of spiral arms may produce similar effects (e.g. Sánchez-Menguiano et al. 2016a, Vogt et al. 2017) without involving the same physics claimed to explain the FMR (i.e., a strong effect of outflows and inflows). Finally, there are authors that have reported the existence of individual regions in galaxies with anomalous metallicities (AMR), that deviate from the rMZR (e.g. Hwang et al. 2018). Like in the case of Sánchez-Menguiano et al. (2019), they consider that gas accretion is the main cause of these deviations. The AMRs are located mostly in interacting systems and in the direction of the close companion, which indeed suggests a non secular origin, different than the concept of the FMR or rFMR (aimed to describe the quiescent evolution of star-forming galaxies in general). So far, with the current compilation of data, the results by Barrera-Ballesteros et al. (2016) are reproduced, showing no significant correlation between the residual of the rMZR with the Σ_{SFR} (i.e., no general/fundamental secondary relation with the SFR is appreciated).

The global and local relations of the oxygen abundance with both M_* and Σ_* are a consequence
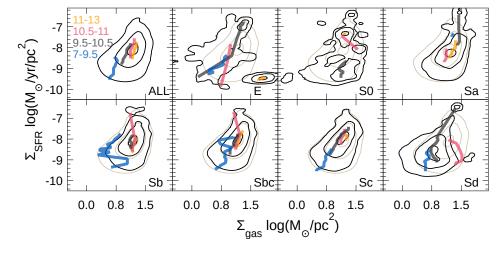
Figure 9

Distribution of the luminosity-weighted metallicities of the stellar populations along the stellar mass surface densities derived from the azimuthal averaged radial distributions described in Sec. 4.7 (Fig. 14 and Fig. 12), for the galaxies considered in this review segregated by stellar mass and morphology. The top-left panel includes the distributions for all the galaxies with different colors indicating different mass ranges and the remaining panels include the same distributions for different morphologies, from earlier (top-left) to later types (bottom right).

of how α elements (O-like) are produced (i.e., expelled to the ISM by type-II SN, the direct by-product of SF). On the other hand, non-α elements (Fe-like), are introduced to the ISM by different mechanisms, involving not only the production of new stars but the death of intermediate mass ones (by the production of type Ia SNe). Indeed, the $[\alpha/Fe]$ ratio is strongly related to the shape of the star-formation histories in galaxies (e.g. de La Rosa et al. 2011). As the SFH changes for galaxies of different mass (e.g. Panter et al. 2003), and morphologies (e.g. López Fernández et al. 2018), and from the inside-out (e.g. Pérez et al. 2013, Ibarra-Medel et al. 2016), the dependence of the stellar metallicity with the stellar mass is less obvious than that of the oxygen abundance. The existence of a global stellar mass-metallicity or M_*-$[Z/H]$ relation in galaxies, summarized in Sec. 3.4, highlights the relation between the shape of the SFH and the stellar mass density (and therefore, the integrated stellar mass too).

A local counter-part of this global relation has not been broadly explored. To our knowledge it was presented in González Delgado et al. (2014a), where they presented the distribution along the Σ_*-$[Z/H]$ diagram for the azimuthal averaged mass-weighted stellar metallicities of 300 galaxies extracted from the CALIFA survey. I present in Fig. 9 a similar distribution for the collection of data adopted here. Following González Delgado et al. (2014a), in order to minimize the scatter introduced by the large uncertainties in the derivation of $[Z/H]$ in individual spectra, I first derive azimuthal average values in bins of 0.1 Re for each galaxy (i.e., I create radial distributions of $[Z/H]$, that I will discuss later, in Sec. 4.7.2). Broadly speaking the results are consistent with those presented by González Delgado et al. (2014a), with the local $[Z/H]$ increasing with Σ_*, in particular for the same stellar mass regime ($M_* > 10^{9.5} M_\odot$, once considered the differences in the adopted IMFs). This agrees with the existence of a negative stellar metallicity gradient in most massive galaxies (e.g. González Delgado et al. 2014b, Oyarzun et al. 2019). However, contrary to what happen with the rMZR, the local stellar metallicity-Σ_* relation is not the same for all galaxies. It depends strongly on galaxy mass and morphology. In

particular, for low-mass and late-type galaxies the distribution of [Z/H] along Σ_* is almost flat or even negative. This indeed agrees with a flattening of the stellar metallicity gradient observed in this kind of galaxies (González Delgado et al. 2014b). In addition, the observed differences between the behaviour of the gas phase (oxygen) and stellar metallicities across galaxies implies a change in the SFHs and therefore a differential chemical enrichment history for α and non-α elements.

4.5. Local star-formation law

Figure 10

Distribution of the star-formation rate surface densities along the gas mass surface densities derived from the azimuthal averaged radial distributions shown in Fig. 15 and Fig. 12 for the galaxies in this review segregated by stellar mass and morphology. I adopted the same nomenclature and symbols used in Fig. 6.

The birth of new stars comprises two different processes. First, the diffuse atomic gas is transformed into high dense molecular gas. Second, stars are born due to the dynamical collapse of self-gravitating portions of those molecular clouds. Schmidt (1959) proposed that the SFR should depend on the mass of gas included in a volume, just assuming that all stars are formed locally from the original available gas, and that there was no inter-exchange (of stars and gas) with the near environment (i.e., $SFR = M_{gas}^n$). However, the power-scaling factor (n) between both quantities was not defined. Kennicutt et al. (1989) proposed that this scaling factor could be derived through the gas free-fall time (τ_{ff}), following the equation $\rho_{SFR} \propto \rho_{gas}/\tau_{ff}$, by assuming that all gas collapsed within this time is transformed into stars. Considering that $\tau_{ff} \propto \rho_{gas}^{-0.5}$, they conjectured that the basic star-formation law should follow a relation $\rho_{SFR} \propto \rho_{gas}^{1.5}$. Empirically, Kennicutt et al. (1989) and Kennicutt (1998a) demonstrated that indeed the surface density of the SFR follows a relation with the gas surface density similar to proposed one. This relation was derived originally galaxy wide, and it is known as the SK-law (Schmidt-Kennicutt law) or star-formation law.

As discussed in previous sections SF, and in particular the collapse of molecular clouds, is a local process that happen at much lower scales than a galaxy size. Spatially-resolved observations have shown that indeed the SK-law is verified only for molecular gas (Wong & Blitz 2002, Kennicutt et al. 2007), a result confirmed for integrated quantities too (e.g. de los Reyes & Kennicutt 2019). At kpc-scales it shows an almost linear relation (e.g. Bigiel et al. 2008, Leroy et al. 2008). Therefore, the

depletion time ($\tau_{dep} = \Sigma_{gas}/\Sigma_{SFR}$) or star-formation efficiency (SFE= $\Sigma_{SFR}/\Sigma_{gas}$) are almost constant at these scales (Bolatto et al. 2008, Hughes et al. 2010), with a value of ~2 Gyr (e.g. Bigiel et al. 2008, Rahman et al. 2012, Leroy et al. 2013). However, these studies are biased towards low-mass, late type galaxies. It is still not known if this result holds in more massive, or more early-type galaxies. The particular conversion factors to derive the molecular gas and the adopted IMF may play a role in these results. It is known that there are clear deviations from the SK-law (thus variations in τ_{dep}) at sub-kpc scales (Schruba et al. 2011, Kruijssen & Longmore 2014, Kruijssen et al. 2019), in extreme starburst galaxies (e.g. Daddi et al. 2010, Genzel et al. 2010), in the center of galaxies (Leroy et al. 2013, Jogee et al. 2005, Utomo et al. 2017), in regions near strong spiral arms or with different local dynamical states (Schruba et al. 2019), and in early type galaxies (Davies et al. 2014). The average τ_{dep} within a galaxy presents a clear dependence with sSFR and M_* (Saintonge et al. 2017). All these results clearly indicate that the combination of the optical spectroscopic information provided by IFS-GS, for a wide variety of galaxies, with estimations of the cold gas content at similar spatial scales is crucial to understand these processes (e.g. Bolatto et al. 2017, Ellison et al., in prep.). It is beyond the scope of this review to make a detailed exploration of the cold gas content in galaxies (atomic or molecular), or to explore the star-forming law at different scales (see Kennicutt & Evans 2012, Bolatto et al. 2013, for detailed reviews on the topic). In this section I just summarize the most recent results based on the combination of IFS data with molecular gas at kiloparsec resolutions.

So far the number of galaxies sampled by both IFS-GS and spatial resolved molecular gas observations is rather small. Pioneering studies cover mostly early-type galaxies observed by the SAURON and Atlas3D surveys (e.g. ~40 galaxies, Alatalo et al. 2013). More recent explorations range from a handful of objects (e.g. Belli et al. 2017, Stark et al. 2018), or a few tens (like the ~47 galaxies in the ALMAQUEST collection, Lin et al. 2017, Ellison et al. in prep.) to a well defined sample of over one hundred galaxies (EDGE-CALIFA sample, Bolatto et al. 2017). There are a few on-going surveys, like PHANGS (Rosolowsky et al. 2019), but they are focused on large galaxies in the Local Universe that can hardly be a representative sample of the $z \sim 0$ population due to the cosmic variance and the limited sampled volume.

To highlight the urgent need of complementary explorations of the molecular gas on a large sample of galaxies already covered by IFS-GS, I present, in Figure 10 the spatially-resolved distribution in the $\Sigma_{SFR} - \Sigma_{gas}$ diagram for the sample of galaxies used in this review. Lacking of spatially resolved information for the molecular gas I adopted the dust-to-gas conversion proposed by Barrera-Ballesteros et al.(in prep., using data from the EDGE-CALIFA survey), already used in **?** and Sánchez et al. (2018). It involves an additional scatter of ~0.3 dex to the relation, but it is the best proxy I can adopt so far. Despite these limitations, there is a clear relation between the two parameters, with a slope near one (α=1.12±0.09), and an average τ_{dep} ~1.7 Gyr, in agreement with published results. The dispersion of the relation, ~0.1 dex, is clearly below the expected individual errors, which validates the approach adopted. When this relation is explored using estimations of the molecular gas based on direct CO observations the scatter is as low as ~0.05 dex (e.g. Bolatto et al. 2017, Lin et al.in prep., Ellison et al. in prep.). Indeed, it is possible that the rSFMS (and the SFMS) are a direct consequence of this relation through a tight $\Sigma_{gas} - \Sigma_*$ ($M_{gas}-M_*$) relation (shown by Lin et al. in prep. and Calette et al. 2018, respectively).

Earlier-type galaxies present shallower relations (α ~0.8-0.9) with a larger dispersion, and larger τ_{dep} (~10 Gyr) than late types, that present steeper slopes (α ~1.2-2.7), smaller dispersion, and lower τ_{dep} (~0.5 Gyr). Both results agree with the most recent explorations by Colombo et al. (2018), Utomo et al. (2017), and Lin et al. (2017) using direct estimations of the molecular gas derived from CO observations, and broadly the model presented by Belfiore et al. (2019a). These results indicate that the ageing and quenching of the star-formation is driven not only by the lack of molecular gas (e.g.

Saintonge et al. 2016), but also by a decline in the SFE (e.g. Sánchez et al. 2018) (i.e., increase in τ_{dep}). The observed differences imply that most probably there is no unique τ_{dep} (or SFE) value or single SK-law for all galaxies and areas within them (e.g., Ellison et al. in prep.), contrary to the early evidence. In other words, τ_{dep} (SFE) may depend on additional parameters whose inclusion in the star-formation law would reduce the scatter in the $\Sigma_{SFR} \propto \Sigma_{gas}$ relation (e.g. Dey et al. 2019, Bluck et al. in prep.).
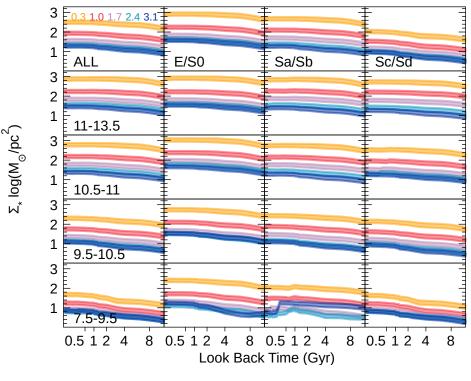
Following this reasoning it is possible to reconcile the observed differences for high-redshift starburst galaxies and nearby disks, and even between the observed differences in the central and outer regions of galaxies. The processes involved would be: (i) the inclusion of the orbital or dynamical time (τ_{dyn}), that connects the gravitational instability (due to bar or spiral arms) with a bursting in the SFE (Silk 1997, Elmegreen 1997); (ii) the gas velocity dispersion as a measurement of the local pressure that increases due to the SF feedback (Silk 1997); (iii) the stellar velocity dispersion, in particular in bulges, that stabilize the molecular clouds preventing the SF (Martig et al. 2009); (iv) the local gravitational potential traced by Σ_* (that would connect the SK-law with the SFMS) (e.g. Saintonge et al. 2011) ; (v) the gas metallicity that facilitates the cooling (e.g. Casado et al. 2015); or (vi) a combination of all of them (e.g. Dey et al. 2019). In summary, the current results indicate that the star-formation law follows the SK-law only at a first order.

Furthermore, considering the SK-law, the SF quenching (either global or local) may be related to a deficit of cold gas. As indicated before, there is a global (and local) M_{gas}-M_* ($\Sigma_{gas} - \Sigma_*$) relation for SFGs (and SF regions). This relation is not verified for early-type galaxies, that present a deficit of neutral (at least molecular) gas with respect to their late-type galaxies counterparts of the same M_* (e.g. Calette et al. 2018, and references there in). This deficit is considered as the primary cause of the global decline of the star-formation rate observed in these objects (e.g. Saintonge et al. 2011). The same deficit is appreciated at local scales, where retired regions present lower Σ_{gas} than star-forming ones at the same Σ_*. With the explored compilation of data I confirm this trend.

The origin of this deficit is still not clear. Several authors consider that it is originated by AGN feedback, either by removing gas due to galactic winds or heating it preventing to collapse and form stars (e.g. Sanders & Mirabel 1996, Hopkins et al. 2009). However, the evidence connecting AGN and quenching is still circumstantial: (i) it seems to be the only process energetic enough to produce this effect (e.g. Croton et al. 2006, Henriques et al. 2019); (ii) their hosts are located in the green valley between SFGs and RGs (e.g. Kauffmann et al. 2003, Sánchez et al. 2004, Schawinski et al. 2014), as indicated in Sec. 3.2, sharing many of their properties with GV galaxies (e.g. Sánchez et al. 2018, , Lacerda in prep.). However, there are still problems in this scenario, like the lack of direct evidence (although see Fabian 2012) and the mismatch of the time scales between quenching (~1-2 Gyr) (e.g. Sánchez et al. 2019a) and the length of an AGN phase (~ 1-2 Myr, e.g. Urry & Padovani 1995). Other authors indicate that the presence of the bulge itself could stabilize the atomic gas preventing it to collapse forming molecular clouds or decreasing the SFE (e.g. Martig et al. 2009). In this case, a decline in the general SFE (and towards the center) could contribute to the halt of the star-formation (or gives support to this halt, as suggested by Bluck et al. in prep). An additional complication is that the presence of an AGN is directly linked with the presence of a bulge through the Magorrian et al. (1998) relation (e.g. Kormendy & Ho 2013). Therefore, a clean distinction between the two processes is difficult.

4.6. Spatially resolved star-formation histories

The analysis adopted in the different publications reviewed in the previous sections exploring the properties of the stellar populations relies on the assumption that the observed spectra of galaxies (and

Figure 11

Distribution of the cumulative stellar mass surface densities at different galactocentric distances (labelled with different colors) along the look-back time for all galaxies with spatially-resolved information (top-left panel), and for galaxies of different morphology (panels from left to right) and/or stellar masses (panels from top to bottom).

regions within galaxies) preserve the imprints of their cosmological evolution, and that these imprints can be used to trace back that evolution. This method is known as the fossil record, and has been reviewed in detail by other authors (e.g. Walcher et al. 2011, Conroy 2013). In particular, Walcher et al. (2011) explore how the main properties of the stellar populations (luminosity and mass weighted ages and metallicities, dust attenuation and masses) can be derived from the decomposition of the stellar continuum (and its limitations).

In principle, from this analysis, it is possible to recover star-formation and chemical-enrichment histories. The fossil record methods have two main implementations. One adopts a particular shape for the SFHs and ChEHs (e.g., Gallazzi et al. 2005, Thomas et al. 2010, Bitsakis et al. 2016, Zibetti et al. 2017), and compare the observed spectra with the predicted ones tuning/fitting certain parameters that govern the functional forms considered: e.g., the decay time of an exponential SFH (τ), or the time delay for the ignition of SF in the Universe (t_{delay}). A second approach consists in a non-parametric exploration of the SFHs (and ChEHs), based on their decomposition in single bursts of SF. Each burst produces a single-stellar population (SSP), a set of stars born all at a certain time (and therefore with the same age as they evolve) from the same gas with a certain metal content (e.g., Panter et al. 2007, Vale Asari et al. 2009, Pérez et al. 2013, Ibarra-Medel et al. 2016, García-Benito et al. 2017). The first approach is unable to reproduce in detail the full spectral features of the observed spectra, and it is frequently used to compare with broad (or medium) band photometry or with particular stellar

features (like stellar indices, e.g. Gallazzi et al. 2005, Zibetti et al. in prep.). However, it provides with SFHs (and ChEHs) that are more easily interpreted. The later approach is able to reproduce the details of the observed spectra, however, the interpretation of the results is frequently less obvious. It is technically complex, and prone to large uncertainties (e.g., Cid Fernandes et al. 2014, Sánchez et al. 2016c). The results depend strongly on the selected templates of SSPs or the stellar libraries (e.g., González Delgado et al. 2014b), and on how the errors propagate when non-linear components are considered, like the dust attenuation or the stellar kinematics (Cid Fernandes et al. 2013, 2014). Finally it relies on the assumption that the SSPs are eigenvectors, which is mathematically not right. Therefore, it may present different degenerancies, like the age-metallicity or the metallicity-velocity dispersion one (e.g. Sánchez-Blázquez et al. 2011). Further issues, involving the IMF assumed, stellar evolution isochrones, stellar template adopted, dust extinction curve, and so on are discussed in detail in Walcher et al. (2011). I should clarify that most of these caveats apply to the parametric methods too.

Using the fossil record method it was possible: (i) to confirm the downsizing in galaxies (e.g., Pérez-González et al. 2008, Thomas et al. 2005, 2010); (ii) to explore cosmic evolution of the SFR density in the Universe (e.g., Panter et al. 2007, López Fernández et al. 2018, Sánchez et al. 2019a) reproducing the distribution derived from direct observations (e.g. Madau et al. 1998, Madau & Dickinson 2014); and (iii) to predict the global chemical enrichment history of galaxies (e.g., Asari et al. 2007). Most of those results were based on single aperture spectroscopic data and/or integrated multi-band photometry, and therefore, they trace the evolution of galaxies as a whole. The advent of IFS-GS has allowed the exploration of the spatially resolved SFHs of galaxies. The pioneering study by Pérez et al. (2013), using a limited sample extracted from the CALIFA survey, first demonstrates that the downsizing is spatially preserved: (i) the central and outer regions of more massive galaxies grow faster than those of less massive ones; (ii) the inner regions of galaxies more massive than $\gtrsim 10^{9.5-10} M_\odot$ assemble their mass faster than the outer regions, following an inside-out growth; (iii) for less massive galaxies there is a possible transition from the inside-out towards the outside-in. Recent updates of these results, using the full CALIFA sample, including UV-photometry and/or adopting a different inversion method were presented in González Delgado et al. (2017), García-Benito et al. (2017) and López Fernández et al. (2018). These results were broadly confirmed with the exploration by Ibarra-Medel et al. (2016) of a much larger sample of galaxies extracted from the MaNGA survey. The main difference reported was that the outside-in regime at low mass was not fully confirmed (a regime not well covered by the original CALIFA sample). In this later work the diversity of spatially resolved SFHs (rSFHs, hereafter) was studied, finding that more massive galaxies present very similar rSFHs at the different spatial regimes explored. However, as the integrated mass decreases, galaxies present a much large variety of rSFHs (what implies a larger dispersion in their average properties, like age and metallicity). However, on average, they follow an outside-in rSFHs, in agreement with the distributions found in the Σ_*-O/H and Σ_*-[Z/H] diagrams (Sec. 4.4). The validity and limitations of this method and the results reported were explored through the analysis of post-processed cosmological hydrodynamics simulations, where the rSFH are well known (Ibarra-Medel et al. 2019).

I reproduce these results in Fig. 11, which shows the average evolution of the stellar mass density at different look-back times and for different radial bins, Σ_*(r,t) for the sample of galaxies explored here. Different panels show the distributions segregated by mass and morphology. Following Pérez et al. (2013) and Ibarra-Medel et al. (2016), the radial bins are selected normalized to the current ($z = 0$) observed effective radius. The figure shows that more massive galaxies indeed present larger values of Σ_*(r,t) than less massive ones at any radius and cosmological time (i.e., the local/resolved downsizing). This segregation is also seen for different morphologies, with earlier type galaxies having larger Σ_*(r,t) than later types, not only at any r and t, but also at any stellar mass bin. Thus, the local

downsizing does not depend only on the mass, but also on the morphology. This result was published by García-Benito et al. (2017), who shows that the local downsizing and inside-out growth has a trend with $\Sigma_{*,cen}$ (the stellar mass density in the center, ~1kpc, of galaxies). Indeed, their results suggest that the diversity in the rSFHs found by Ibarra-Medel et al. (2016) for low-mass galaxies has a clear dependence with this parameter.
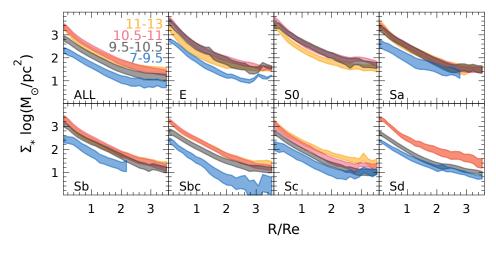
García-Benito et al. (2017) reported two additional results: (i) the scale-length of galaxies in mass is smaller (on average) than the corresponding parameter in light (characterized by r_{50}). This result, already shown in González Delgado et al. (2014b), indicates that galaxies grow faster in mass than in light. Although I do not show a similar plot, this result is clearly reproduced with the sample explored in this review; (ii) the local downsizing (understood as the speed of mass assembly) with morphology maybe be broken for E/S0, which seem to form their outer regions at a slower rate than Sa. A possible explanation is that in early-type galaxies captures/minor mergers affect the mass-assembling history in the outer regions, resembling a change in the local downsizing, as proposed by Oyarzun et al. (2019). Further explorations, and in particular deep comparisons with mock/simulated galaxies (following Ibarra-Medel et al. 2019) are required to fully understand all these results.

4.7. Radial gradients of galaxy properties

It is clear that the properties of the stellar populations and ionized gas change along the optical extensions of galaxies, showing patterns and relations that reassemble well-known ones derived for integrated properties. In many cases the explored physical parameter (Σ_{SFR}, Age, [Z/H], O/H, or Σ_{gas}), present clear dependencies with Σ_*. As this parameter present a clear radial trend in galaxies (e.g. González Delgado et al. 2014b), it is expected that many of the analyzed parameters present radial trends too (e.g. Barrera-Ballesteros et al. 2016). Beside this radial trends, due to the different substructures observed in (late-type) galaxies, like spiral arms and bars, azimuthal or local deviations from the pure radial distribution are expected (e.g. Sánchez-Menguiano et al. 2016a). In this section I review the most recent results regarding the radial distribution of the spectroscopic properties of galaxies and their relation with the observed patterns described in previous sections.

Along this review all radial distributions are shown with distances normalized to the effective radius of each galaxy (R_e, already used in Fig. 5). I adopt this scheme instead of representing them in physical scales since this way it is possible to compare with galaxies covering a wide range of sizes. This method was introduced by Sánchez et al. (2012b) and nowadays is commonly used (e.g. González Delgado et al. 2014b, 2015, 2016, Sánchez-Menguiano et al. 2016b, Belfiore et al. 2017c, Sánchez-Menguiano et al. 2018), since it does uncover patterns not clearly seen when using physical sizes (e.g. Pérez et al. 2013, Ibarra-Medel et al. 2016). Moreover, the effective radius has been proved to be really effective, with most of the physical parameters sampled at this distance being representative of the average values across the optical extension of galaxies (e.g. Moustakas & Kennicutt 2006, Sánchez et al. 2013, González Delgado et al. 2014b).

4.7.1. Stellar mass density gradients.
It is well known that the radial distribution of the azimuthal averaged surface brightness profiles (SBP) present an almost monotonic decrease for almost all galaxy types of any stellar mass. In the case of disk-dominated spiral-like galaxies this profile is well characterized, as a first order, by an exponential function of the radius (Freeman 1970) or a double exponential profile (e.g. Courteau et al. 1996). On the other hand, the SBP of early-type galaxies (or the bulge of late-type ones) is better represented by a sharper profile, well described by an exponential of the 1/4th power of the radius (de Vaucouleurs 1959), or a more general profile known as the Sersic profile (Sersic 1968), characterized by the power of the radius known as the Sersic index (n_s).

Figure 12

Azimuthal-averaged radial distributions of the stellar mass surface density for the galaxies in this review segregated by stellar mass and morphology (as indicated in the inset). The top-left panel includes the radial distributions for all the galaxies with different colors indicating different mass ranges and the remaining panels include the same distributions for different morphologies, from earlier (top-left) to later types (bottom right).
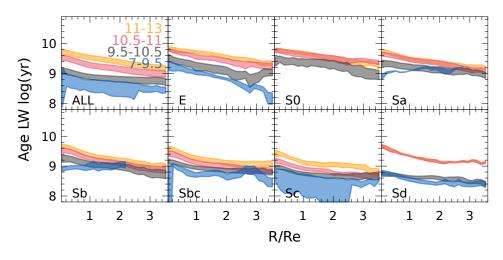
In general, early-type spirals (Sa/Sb) require a combination of a single or a double exponential plus one of the functional forms described to characterize the bulge. The description of other structural components, like a bar, requires the inclusion of further functional forms (e.g. Méndez-Abreu et al. 2017, and references therein). Irregular or interacting galaxies show much complex radial profiles and in many cases their characterization requires a full analysis of the two-dimensional distribution using more complicated functional forms (e.g. Peng et al. 2010, Méndez-Abreu et al. 2017).

The radial decline of the SBP is nowadays accepted to be a consequence of an almost monotonic decline in the stellar mass density (Σ_*), via a conversion through the M/L-ratio (e.g. Bakos et al. 2008). In general, the M/L-ratio presents a log-linear relation with optical colors, a simple consequence of the color-age relation in stellar populations (e.g. Bell & de Jong 2001, Zibetti et al. 2009). As galaxies contain older stellar populations in their central regions (e.g. González Delgado et al. 2014b), the M/L-ratio enhances the radial decline of Σ_* with respect to that of the SBP. For this reason the R_e in light is larger, in general, than the one derived in mass (as indicated in the previous section). The advent of IFS-GS has allowed to explore the spatially resolved distribution of the stellar population content, providing with more accurate M/L-ratios at kilo-parsec scales (e.g. García-Benito et al. 2019). This improves the derivations based on colors (e.g. Bell & de Jong 2001), adopted in previous studies (e.g. Bakos et al. 2008). These new datasets facilitate the systematic exploration of the radial distributions of Σ_* in galaxies of different morphology and stellar mass.

Figure 12 shows the radial distribution of Σ_* for the current adopted compilation. As stated beforehand all galaxies, irrespective of their morphology and mass, present a decline of Σ_* with radius. The central ($\Sigma_{*,cen}$) and effective ($\Sigma_{*,Re}$) stellar mass densities increases with the integrated mass and morphology (as they become earlier) for galaxies later than S0s. González Delgado et al. (2014b) already shown that Elliptical galaxies, are more compact, with a steeper radial decrease of Σ_*, in particular more massive ones. Note that when the radial distribution of Σ_* is not normalized by R_e, the picture changes, since there is a correlation between M_* and R_e (e.g. Cappellari 2016, van de Sande

et al. 2019).

González Delgado et al. (2014b) showed that galaxies, in general, present two regimes in the radial distribution of Σ_*, one at $R < 0.5R_e$, steeper (with a slope ranging between $\alpha \sim -0.5$ dex/Re and ~ -1.5 dex/Re), and another one at $R > 0.5R_e$ (with an almost constant slope of $\alpha \sim -0.5$ dex/Re). The first one corresponds (broadly) to the bulge, while the later one corresponds to the disk (for late-type galaxies). Finally, the radial profile is steeper (~ -1.5 dex/Re) for more massive galaxies and shallower for less massive ones (~ -0.5 dex/Re). All these trends are qualitatively appreciated in Fig. 12. They agree with the explorations of the rSFHs reviewed in previous sections: the stellar mass assembles faster and with stronger intensities (higher SFRs) in the inner regions of more massive/early-type galaxies than in the outer-regions of less massive/late-type ones.
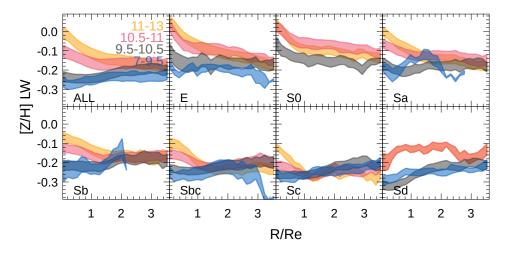

Figure 13

Azimuthal-averaged radial distributions of the luminosity-weighted stellar ages for the galaxies in this review segregated by stellar mass and morphology; colors and symbols as in Fig. 12.

4.7.2. Stellar age and metallity gradients. Pioneering works on the radial gradients of colors and stellar indices were already performed four decades ago (e.g. Faber 1977). Radial changes in both properties were interpreted as a physical variation in the average ages (and metallicities) of the stellar populations. The combination of better quality long-slit spectroscopy with broad-band imaging, focused on the study of elliptical galaxies (e.g. Peletier et al. 1990, González 1994), shows that they present a shallow gradient in age and a clear negative gradient in metallicity. These early results were revisited based on the analysis of larger samples of galaxies, using multi-broad band photometry, long-slit and even IFS data (e.g. Mehlert et al. 2003, Sánchez-Blázquez et al. 2007, Rawle et al. 2008, Coccato et al. 2010, Kuntschner et al. 2010, Spolaor et al. 2010, Koleva et al. 2011, McDermid et al. 2015, González Delgado et al. 2014b, 2015, Goddard et al. 2017, Ruiz-Lara et al. 2016, Oyarzun et al. 2019). All these studies agreed on reporting a negative gradient in the stellar metallicity, [Z/H], but the consensus was less clear for the presence of a negative age gradient. Goddard et al. (2017) reported a flat or even a positive gradient in the stellar ages of early-type galaxies, explained by an "outside-in" scenario, based on data extracted from the primary sample of the MaNGA survey (reaching 1.5 R_e). Similar positive age gradients are sometimes described from analysis based on broad-band colors (e.g. Tortora et al. 2010). In spectroscopic based studies clear positive age gradients were found before only

in the very central regions (~Re/8 Kuntschner 2015, McDermid et al. 2015). At larger scales, different authors have found contradictory results. They either found a wide range of gradients, from negative to positive (e.g. Spolaor et al. 2010, Koleva et al. 2011) or shallow negative gradients or absence of a gradient (e.g. Sánchez-Blázquez et al. 2007, Rawle et al. 2010). However, when the spectroscopic data reach the outer regions of galaxies (R>2 R_e), most of the studies report a negative gradient in the stellar ages supporting an "inside-out" scenario (e.g. González Delgado et al. 2014b, Li et al. 2015, González Delgado et al. 2015, Zheng et al. 2017).

Figure 13 shows the radial gradients of the luminosity-weighted ages derived using our own analysis based on our compilation of IFS observations. For early-type galaxies of any mass there is a clear negative gradient, in agreement with most of the published results, although I should stress that there is no full consensus in this regard. The lack of consensus is deeply ingrained in the procedure adopted to derive the stellar ages. González Delgado et al. (2014b) and González Delgado et al. (2015) used a full spectral fitting based on the STARLIGHT code (Cid Fernandes et al. 2011). This code, like PIPE3D implemented in this review, uses the full optical spectral range and does not removes the shape of the spectral continuum (i.e., features like D4000 are important in that derivation), contrary to the one adopted by Goddard et al. (2017). Removing the shape has strong implications, since the dust attenuation is no longer recovered (although not removing it requires a high quality spectrophotometric calibration Walcher et al. 2011). Recent results show that the polynomial functions adopted in some methods to describe and correct the shape are indeed very similar to the expected correction by a dust attenuation law (Belfiore et al. 2019b). Finally, I should indicate that the use of different wavelength ranges (e.g., Atlas3D covers just the wavelength range between 4800-5380Å, Cappellari et al. 2011), or the inclusion or exclusion of the alpha-enhancement in the models could contribute significantly to the reported differences.

Figure 14

Azimuthal-averaged radial distributions of the luminosity-weighted stellar metallicities ([Z/H]) for the galaxies in this review segregated by stellar mass and morphology; colors and symbols as in Fig. 12.

The number of similar studies for late-type galaxies is limited. This is mostly due to the difficulty of removing the emission lines that contaminate the spectra, in particularly important ranges, like the regions covered by the Balmer absorption lines (sensitive mostly to the age, e.g., Worthey 1994). Different fitting techniques have addressed this issue in different ways (e.g. Sarzi et al. 2006,

Sánchez-Blázquez et al. 2014b, Sánchez et al. 2016c), removing efficiently this contamination. In this regard the consensus is that the averaged ages of the stellar populations present a negative gradient for all late-type galaxies more massive than $10^{9.5}M_\odot$, with a somehow similar slope (Sánchez-Blázquez et al. 2014a, González Delgado et al. 2015, Goddard et al. 2017, Ruiz-Lara et al. 2017). The stellar metallicity presents a negative gradient only for earlier-type spirals (Sa,Sb,Sbc) and more massive ones ($M_* > 10^{9.5}M_\odot$), with a slope that becomes shallower for low-mass and late-type galaxies. This is illustrated in Figure 14, which shows the radial gradients of the luminosity weighted stellar metallicities derived for our data compilation. Again, these results agree with the scenario reviewed in Sec. 4.6, with an "inside-out" growth for more massive and earlier-type galaxies, and an "outside-in" growth, for the less massive and later-type ones.

However, we should be cautious for the low-mass/later-type galaxies. For galaxies with strong star-formation with respect to their mass (i.e., the low mass SFGs, mostly Sc and Sd, with high sSFR) that are more metal poor ones (following the MZR), the estimation of age and metallicity is highly degenerated. The degeneracy between these two parameters is well known and widely studied (e.g. Walcher et al. 2011). However, in this range it is far more complicated: (i) the presence of strong emission lines on top of the Balmer absorptions in combination with the fact that the spectral features are narrower due to the combination of the type of stars and the low velocity dispersion, affects the accuracy in the removal of the contamination by the emission lines; (ii) the absorptions by metallic elements are weaker than in the case of more massive galaxies, making it more difficult to obtain a precise metallicity; (iii) this, in combination with the limited range of values for the 4000Å break when the light of the stellar population is dominated by young stars, affects the accuracy and precision in the derivation of both ages and metallicities.
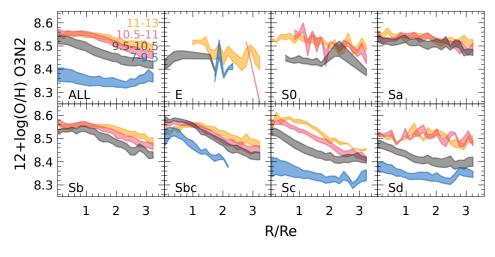
4.7.3. Oxygen abundance gradients.

Before the stellar population analysis had enough accuracy to explore the metallicity gradients in SFGs, for decades, the study of the chemical enrichment was based in the analysis of the gas-phase abundance. In particular H II regions have been considered as good tracers of the chemical composition in these galaxies. It was already in the seventies of the past century that the presence of a negative abundance gradient across the discs of nearby galaxies had been uncovered (Searle 1971, Comte 1975), even in the Milky Way (MW, Peimbert et al. 1978). This gradient has been confirmed by different observations (e.g. Matteucci & Francois 1989, Vila-Costas & Edmunds 1992, Martin & Roy 1994, Zaritsky et al. 1994, Esteban & García-Rojas 2018), and some deviations from this single negative gradient have been appreciated (Belley & Roy 1992, Vilchez & Esteban 1996, Roy & Walsh 1997). Like in the case of other gradients explored in this review, the use of the effective radius as a scale-length has helped to uncover the patterns and differences between galaxy types. Diaz (1989), and later Vila-Costas & Edmunds (1992), demonstrated that using a scale-length anchored to the galaxy properties (like R_e and R_{25}), instead of a pure physical radial distance, reduces the scatter in the distribution of slopes of the abundance gradients. Following this philosophy, with the advent of large IFS observations, Sánchez et al. (2012a) and Sánchez et al. (2014), showed that all star-forming galaxies more massive than $M_* > 10^{9.5}M_\odot$, present a characteristic oxygen abundance gradient of ~ -0.1 dex/R_e when computed within the range between 0.5-2.0 R_e (i.e., the disk region). Contrary to early results (e.g. Zaritsky et al. 1994) the slope of the gradient in this region does not seem to be strongly affected by other properties of the galaxy, like morphology or the presence of a bar. This result was confirmed also for the stellar metallicity (Sánchez-Blázquez et al. 2014a).

Besides the presence of a common/characteristic gradient, for some galaxies there is an apparent flattening or drop of the abundance in the central regions (R<0.5 R_e), and a flattening in the outer regions (R>2 R_e) for all the galaxies analyzed. These results were confirmed using larger IFS datasets (e.g. Sánchez-Menguiano et al. 2016b, Zinchenko et al. 2016, Pérez-Montero 2017, Belfiore et al.

R$_{25}$: radius of the elliptical isophote of a galaxy at which it is reached a surface-brightness of 25 mag arcsec^2 in the V-band.

Characteristic gradient: oxygen abundance presents similar slopes in their gradients for disk galaxies with $M_* > 10^{9.5}M_\odot$.

Figure 15

Azimuthal-averaged radial distributions of the gas-phase oxygen abundances derived using the O3N2 calibrator for the galaxies in this review segregated by stellar mass and morphology; colors and symbols as in Fig. 12.

2017c, Poetrodjojo et al. 2018) or observations with exquisite spatial resolution (i.e., MUSE data, Sánchez-Menguiano et al. 2018). Some works described a continuous change in the abundance gradient from almost flat for low-mass galaxies $M_* <10^9 M_\odot$ towards the described characteristic slope, reached at $M_* \sim 10^9 M_\odot$ (Bresolin & Kennicutt 2015, Belfiore et al. 2017c). In other cases no drop or flatenning is appreciated at any scale, and a single slope for the abundance gradient seem to reproduce the data (Pilyugin et al. 2014). The actual selection of the star-forming regions used to derive the gradient may affect somehow the results. For example, the inner drop is not detected when the SF/H ɪɪ regions in the intermediate area between the Kauffmann and Kewley curves are excluded (e.g. Zinchenko et al. 2016). I should stress here that selecting just regions below the Kauffmann (or Kewley) curve may exclude star-forming regions with large forbidden line ratios (i.e., nitrogen enhanced), like the ones described in the inner region of galaxies by Kennicutt et al. (1989), Ho et al. (2014) and Sánchez et al. (2012a). The nature of those regions is still not clear, but they are easily identified as ionized nebulae in narrow-band images or emission line maps based on IFS data.
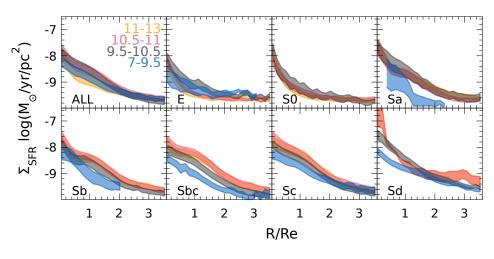
Figure 15 shows the radial profiles of the oxygen abundance for the sample analyzed in this review, segregated by mass and morphology. These profiles reproduce the results reported in the literature well, in particular those by Sánchez-Menguiano et al. (2018). This article presented the most detailed analysis so far on the shape of abundance gradient. It used the super-high resolution data obtained by MUSE, on a sample of more than 100 galaxies, confirming that the slope of the abundance gradient in the disk regime is indeed very similar for all galaxies when the distribution is normalized to the effective radius (as suggested by Sánchez et al. 2014). Regarding the shape, it may present either a single slope, or the combination of a monotonic decrease with either an inner drop and an outer flatenning. Sánchez-Menguiano et al. (2016b) and Belfiore et al. (2017c) already showed that the inner drop is ubiquitous in massive galaxies ($M_* >10^{10} M_\odot$), and not present in low-mass ones ($M_* <10^{9.5} M_\odot$). This is seen Fig. 15, in particular for Sb to Sc galaxies. The effect of radial migration towards the Lindblad resonances, or the freezing of the chemical enrichment associated with the quenching of the star-formation in the inner (bulge dominated) regions are plausible explanations for this deviation from the monotonic decrease. On the other hand, the outer flatenning does not seem to

have a clear pattern. It does not be directly connected with the shape of the surface brightness profile of disk galaxies (e.g. Marino et al. 2016). A change in the efficiency of the star-formation in the outer regions of the disk (e.g. Thilker et al. 2007), or outer radial migrations, are possible explanations to this change in the shape of the abundance gradient (e.g. Bresolin 2017). Sánchez-Menguiano et al. (2018) present the concept of a chemical enrichment scale-length in a galaxy ($R_{O/H}$), defined as the distance at which the oxygen abundance decreases by ~0.1 dex. They show that this parameter presents a linear and almost one-to-one correlation with the effective radius. This relation was already outlined by Bresolin & Kennicutt (2015), when they showed the relation between the slope (in physical scales for the galactocentric disances) and the scale-length of the disk. As a consequence, when normalized by this scale-length the inner drop and the outer flatenning happens virtually at $0.5R_{O/H}$ and $2.0\ R_{O/H}$ for all galaxies, with a very narrow scatter.

Some recent results have questioned the existence of a characteristic abundance gradient. Belfiore et al. (2017c), using data from the MaNGA survey, showed that for some O/H calibrators (Maiolino et al. 2008) there is a strong dependence of the gradient with the stellar mass, with low-mass galaxies ($M_* < 10^{9.5} M_\odot$) presenting an almost flat abundance gradient. However, for other calibrators (Pettini & Pagel 2004) the distribution is consistent with a single slope for most of the galaxies. Poetrodjojo et al. (2018), using data from the SAMI survey, reported a weak trend with the mass only when using an R23-based oxygen abundance calibrator (like the one proposed by Maiolino et al. 2008). For other calibrators, they found an almost constant slope. Moreover, as indicated before, the analysis by Sánchez-Menguiano et al. (2018), using MUSE data (with much better spatial resolution), does not provide any evidence of a dependence of the slope with M_*. In the regime of low-mass galaxies (down to $M_* < 10^{8.5} M_\odot$), the most recent explorations have not found any dependence with M_* either (Bresolin 2019). Thus, the possible dependence with the stellar mass has been reported only for low-mass galaxies, for particular calibrators, and using IFS data of low spatial resolution.

The existence of a general rMZR, discussed in Sec. 4.4, can explain the observed oxygen abundance gradients in galaxies simply considering the existence of an inverse radial gradient in the Σ_*, (Sec. 4.7.1). Indeed, Barrera-Ballesteros et al. (2016) was able to reproduce not only the negative abundance gradient but also the characteristic slope of the gradient in disk galaxies (~ -0.1 dex/Re). The small scatter in the rMZR relation ($\sim$0.05-0.07 dex) and the abundance gradients strongly supports the idea that oxygen chemical enrichment is dominated by local processes, being tightly related to the local star-formation history, without little effects of migrations or mixing beyond few kiloparsecs. This supports the idea that the radial-mixing scale (introduced by Sánchez et al. 2015a, , based on the scatter of the abundance gradient), the typical distance of oxygen abundance mixing in a galaxy, is rather small ($\sim$0.3-0.4 r_e).

In addition to the exploration of the radial gradient of the oxygen abundance, recent studies have been focused on the exploration of possible azimuthal variations in the oxygen abundance. These variations could be induced by the nature of spiral arms as possible density waves, that may produce a differential star-formation history (e.g. Grand et al. 2016, Peterken et al. 2018) with respect to the rest of the disk, and introduce an azimuthal variation in the stellar or gas metallicity. Bars could also induce radial motions that produce azimuthal variations in these physical parameters (e.g. Athanassoula 1992, Minchev et al. 2012, Di Matteo et al. 2013). Pioneering observations have found that the abundance gradient shows subtle differences when the galaxy is divided in quadrants (Rosales-Ortega et al. 2011). More recent studies have found significant azimuthal variations in the oxygen abundance in a handful of galaxies (e.g. Li et al. 2013, Sánchez et al. 2015a, Zinchenko et al. 2016, Sánchez-Menguiano et al. 2016a, Ho et al. 2017, Vogt et al. 2017, Ho et al. 2018). However, when making a statistical analysis there are very little differences, even when considering barred and unbarred galaxies (Sánchez-Menguiano et al. 2016b, Zinchenko et al. 2016). An alternative interpretation is that the observed

azimuthal variations are induced by the presence of anomalous abundance regions (Hwang et al. 2018), more related to gas inflow than to secular processes (Sánchez-Menguiano et al. 2019). In any case, azimuthal variations may be present in some galaxies induced by the combination of very particular dynamical processes or even external effects. However, it seems to have a subtle effect in the radial abundance gradient.

While there are several studies of the oxygen abundance gradients in nearby star-forming galaxies, the systematic studies of nitrogen abundances (N/H) or nitrogen-to-oxygen abundances (N/O) are less numerous. In general, these studies have found a steady monotonic decrease of the N/O ratio from the inner to the outer regions (Pérez-Montero 2014, Belfiore et al. 2017c). There are no significant deviations from this pattern described in the literature. In general it is accepted that most of the Nitrogen observed in galaxies in the nearby universe is due to secondary production, at least for galaxies more massive than $M_* > 10^{9.5} M_\odot$. Thus the N/O gradient follows the oxygen abundance one in general (e.g. Belfiore et al. 2017c).
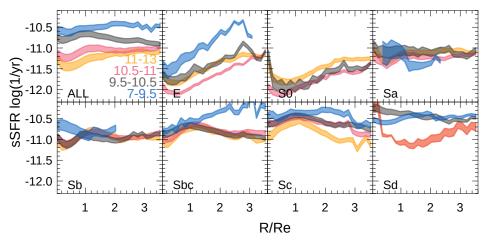

Figure 16

Azimuthal-averaged radial distributions of the surface density of the SFR derived from the Hα intensity for the sample of galaxies, segregated by stellar mass and morphology; colors and symbols as in Fig. 12.

4.7.4. Star-formation rate gradients. The presence of a monotonic decrease of the gas phase oxygen and nitrogen abundances in star-forming (disk mostly) galaxies, described in the previous section, has been interpreted as a direct evidence of an inside-out formation of these objects (Matteucci & Francois 1989, Boissier & Prantzos 1999). Under this scenario the gradient is formed as a consequence of the increased timescales of the gas infall with galactocentric distance. The differential amount of gas supply in the inner regions compared to that of the outer ones implies a differential SFR, assuming a constant or similar depletion time across the disk (i.e., a common S-K law Schmidt 1959, Kennicutt et al. 1989). The subsequent differential chemical enrichment naturally explains the oxygen (and nitrogen) abundance gradients. Most chemical abundance codes aimed to reproduce the described gradients, in particular those in our Galaxy, are based on this scheme on a first order (e.g. Mollá & Díaz 2005, Tissera et al. 2013, Carigi et al. 2019). In summary, this scenario predicts and requires the existence of a monotonic decrease of the star-formation with the galactocentric distance.

Figure 16 shows the radial distribution of the SFR density (Σ_{SFR}). There is a clear peak in the cen-

tral regions with a decrease towards the outer ones, broadly in agreement with the proposed inside-out scenario. González Delgado et al. (2016) was one of the first studies exploring the radial dependence of the star-formation with both the stellar mass and morphology of galaxies. They found results qualitatively similar to the ones presented in Fig. 16. Besides the radial decline in the Σ_{SFR} for all galaxies, early-type galaxies (E/S0) present lower values of star-formation than the ones seen in late-type counterparts at any stellar mass, for any galactocentric distance. Thus, in these galaxies the decline of the star-formation happens at every radial distance. However, the maximum decline is found in the central regions. As already indicated in previous sections, the star-formation activity in early-type galaxies is a somewhat recent topic (see Sec. 4.1), being explored using IFS by a very few number of studies (e.g. Gomes et al. 2016b). In general, these galaxies host less number of star-forming areas, and those star-forming areas are forming stars at a lower rate with respect to those in late-type galaxies (e.g. Cano-Díaz et al. 2019).
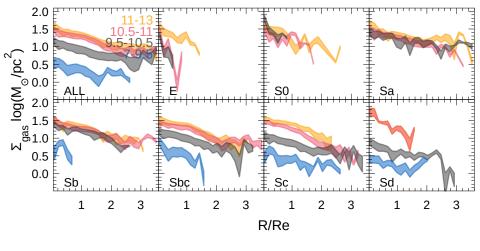
For late-type galaxies (LTGs), the most common morphological type among SFGs, Σ_{SFR} is 0.5-1 dex stronger than that of early-types at any galactocentric distance. Among them, there is a clear variation with the stellar mass and the morphology: more massive and later LTGs present stronger SFRs. However, once normalized by the stellar mass density (Σ_*), the differences are less evident. Figure 17 shows the radial distribution of the spatially-resolved specific SFRs (= $\frac{\Sigma_{SFR}}{\Sigma_*}$). For LTGs (from Sa to Sc), the sSFR presents a very similar value of about $\sim 10^{-11} \mathrm{yr}^{-1}$, with a possible variation of 0.2 dex between earlier and later spirals (in agreement with González Delgado et al. 2016, Belfiore et al. 2017a, Sánchez et al. 2018). The sSFR has units of the inverse of time, and indeed it inverse could be interpreted as the amount of time required to form the current stellar mass at the current SFR (e.g. González Delgado et al. 2016). In purity, this is true if the current observed M_* is corrected by the mass locked in dead stars along cosmological times. However, that correction has a maximum of $\sim$30%, for the adopted IMF (e.g. Courteau et al. 2014). Therefore, it does not affect significantly the order of magnitude of the estimation. This result indicates that at the current Σ_{SFR} galaxies would require hundreds of Gyr to form their current Σ_* (being particularly true for the early-type galaxies). Thus, the SFR in the past must have been considerably higher than today, at any galactocentric distance. This

is in agreement with the observations of the evolution of the SFR along the time based on integrated quantities (e.g. Speagle et al. 2014), or by the exploration of the cosmic star-formation density in the universe (Madau & Dickinson 2014, Driver et al. 2017, Sánchez et al. 2019a).

The low dispersion of the sSFR at any galactocentric distance for late-type (mostly SF) galaxies was interpreted by González Delgado et al. (2016) as a direct consequence of the existence of the rSFMS. Just comparing the radial distributions of the two involved quantities, Σ_* (Fig. 12) and Σ_{SFR} (Fig. 16), it is clear that a rSFMS should hold. Contrary to late-type galaxies, early-type (E/S0) ones exhibit a clear decrease of the sSFR towards the inner regions, at any mass, despite the peak observed in Σ_{SFR} for these galaxies. This has been interpreted by different authors as a clear evidence of an inside-out quenching (González Delgado et al. 2016, Belfiore et al. 2017a, Lin et al. 2017, Ellison et al. 2018, Sánchez et al. 2018). that is evidently related to the presence or influence of a bulge in the halting of the SF activity, either directly (e.g. Martig et al. 2009), or by hosting an AGN. In terms of their distribution along the $\Sigma_{SFR} - \Sigma_*$, early type galaxies, dominated by retired areas, are located well below the loci of the rSFMS (Cano-Díaz et al. 2019, and Fig. 7).

Figure 18

Azimuthal-averaged radial distributions of the surface density of the gas mass estimated based on the dust-to-gas ratio for the galaxies in this review segregated by stellar mass and morphology; colors and symbols as in Fig. 12.

4.7.5. Gas mass density gradients. The exploration of the radial distribution of Σ_{gas} and its connection with Σ_{SFR} (through the SFE) are giving us clues of how the SF is maintained (or enhanced) and the reason for its quenching. In Sec. 4.5 I described the few cases of galaxies covered by IFS-GS and spatially-resolved molecular gas observations. Regarding the radial distribution, the molecular gas content peaks softly in the inner regions (Bolatto et al. 2017, Lin et al. 2017), with a more or less monotonic decrease from the central regions outwards (e.g. Colombo et al. 2018, Fig. 4), with a scale-length (effective or half-light radius) that matches well that of the stellar light (e.g. Bolatto et al. 2017, , Fig. 13), confirming the results by previous studies (Regan et al. 2001, Davis et al. 2013). Figure 18 shows the radial distribution of the molecular gas surface density derived using the dust-to-gas proxy described before (Sec. 4.5) for the well-resolved galaxies in our IFS compilation. The general radial decline reported in the literature is clearly reproduced.

I segregate the radial distributions by stellar mass and morphology, following the scheme of previ-

ous figures. In general, the gas surface density strongly depends on the total stellar mass for late-type galaxies (e.g. Saintonge et al. 2011). However, for early-type galaxies (E,S0 and Sa), there is no clear trend with the mass, in agreement with the results by Young et al. (2011). In addition, for the same mass galaxies of different morphology present similar radial gradients of Σ_{gas}, as reported by Colombo et al. (2018). Finally, the molecular gas fraction decreases for earlier and more massive galaxies. This decline is stronger in the inner regions, as it is evident when comparing the distributions shown in Fig. 12 and Fig. 18. This seems to indicate that the observed decline in the sSFR from the inside-out (Fig. 17) is due primarily to a relative lack of molecular gas. However, a change in the SFE also may play a role.
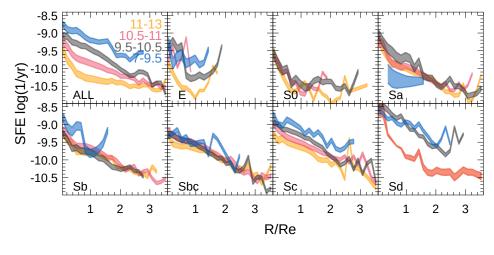
Utomo et al. (2017) found that, on average, the radial distribution of the depletion time τ_d (the inverse of the SFE) is rather flat when analyzed spaxel by spaxel at a kpc-scale. However, this quantity presents a clear radial trend, when radial averages are considered, as shown by Colombo et al. (2018). In the inner regions τ_d has lower values, of the order of ~1 Gyr (SFE~10^{-9}yr^{-1}), and up to ~10-20 Gyr (SFE~$10^{-10.5}$yr^{-1}) in the outer ones, with a clear segregation by mass and morphology (e.g., Fig. 4 of their article). Despite the different proxies adopted to derive the molecular gas mass (dust attenuation vs. CO observations), similar results are recovered for our dataset. Figure 19 shows the radial distribution of the SFE segregated by stellar mass and morphology. The monotonic decrease from the center outwards is clearly shown, with more massive galaxies presenting lower SFE (larger τ_d) than less massive ones. When segregating by morphology the picture is less clear. While for some morphological types (e.g., E or Sc) there is still a segregation by mass, for other ones (e.g., S0 or Sbc) its seems that all galaxies have a similar SFE distribution respective of their mass, without a clear pattern. However, when comparing galaxies of different morphology and the same stellar mass the trend is clear: in general, later galaxies present larger SFE (shorter τ_d) than earlier ones, at any galactocentric distance. Recent results (Ellison et al., in prep.), indicates that this change in the SFE is one of the causes of the dispersion in the rSFMS, that can be observed as a segregation by morphology (e.g. Cano-Díaz et al. 2019). If τ_d is interpreted as the time required to consume the current molecular gas mass with the current SFR, then this time is shorter in the inner regions of less massive and later galaxies and in in the outer regions of more massive and earlier galaxies.

I should note that the reported distributions may change in the presence of bars, that are known to induce radial movements of gas (e.g. Shlosman et al. 1989, Boone et al. 2007, Knapen et al. 2019), and in particular they can produce an increase of the molecular gas and even the SFE in the inner regions of galaxies (in contrast with what is found in here).

5. What we have learned?

Along this review I summarised the most recent results in the characterisation of the spatially-resolved spectroscopic properties of galaxies in the nearby universe (z <0.1). For doing so, I compile the largest possible sample of galaxy data observed using IFS, and replicate the published results (to a certain extend).

In summary, recent results have found that the evolution of galaxies is governed by local properties, but influenced somehow by global ones. The duty-cycle of gas-to-stars, the chemical enrichment, and the quenching and halting of both follow local/spatially resolved scaling/evolutionary laws that are verified at kiloparsec scales in galaxies. Among them, the SK-law, rSFMS and rMZR relations, verified for star-forming regions in galaxies, are followed by regions of different galaxies that to some extent follow the same resolved SFHs and ChEHs. These evolutionary sequences depend both on the galactocentric distance, the stellar mass, and morphology, indicating that most probably they actually depend on the local strength of the gravitational potential and the dynamical/orbital structure. The

Figure 19

Azimuthal-averaged radial distributions of the star-formation efficiency for the galaxies considered in this review segregated by stellar mass and morphology; colors and symbols as in Fig. 12.

central regions of more massive and earlier-type galaxies evolve faster, showing sharper SFHs, initiated by a steady and rapid increase of the SFR, that last less than 1 Gyr, reaching a peak followed by a sharp decay. The outer regions of less massive and later-type galaxies evolve in a slower fashion, with smoother SFHs, initiated with a slow increase of the SFR, reaching its peak of SF at much recent cosmological times (in some cases, they are still in the rising phase of the SF). This, together with a narrow range of depletion times (within a factor ~2) across galaxy types, galactocentric distances, and final stellar masses, explain the observed local relations.

The SFHs shapes the ChEHs, that in general is governed by local processes, with recycling, inflow, and outflow happening more at local than at global scales. The SFHs and ChEHs shape or are shaped by the scaling relations indicated before, that evolves with cosmological times (in the case of the rSFMS and rMZR) or are rather constant (SK-law). Above the kiloparsec scale, integrated/averaged through the optical extension of galaxies, the local/resolved relations are observed as global ones (SFMS, MZR). In some cases, depending on the fraction of regions actually forming stars within a galaxy, the global relations may present shallower relations than the local ones (e.g., SFMS vs. rSFMS). However, not all global relations are induced by local ones. This is the case of the stellar MZR, that relates the average [Z/H] and the stellar mass. There is no parallel Σ_*-[Z/H], since the stellar metallicity depends both on the amount of generated stars and the way that these stars are formed: i.e, both the strength and shape of the SFH. Moreover, a certain time is required before intermediate-mass stars pollute the ISM with non-alpha (Fe-like) elements, and therefore, different SFHs leading to the same Σ_* imply different [Z/H] values.

The described relations shape the radial gradients observed in many different quantities, as a pure consequence of the radial gradient of Σ_*, that is formed in early cosmological times. It seems that the early evolution is dominated by the trigger of SF happening at the same time across galaxies, consuming the gas reservoir that is larger in the central regions by a pure effect of the shape of the gravitational potential. The ignition of the SF, following a SK-law shaped by the free-fall time of collapsing molecular clouds, automatically creates a radial gradient in Σ_*. Due to the local relations indicated before and the differential evolution of the stellar populations (formed faster and earlier in

the central regions of more massive galaxies), the observed properties of galaxies present clear radial gradients with central regions having older and more metal-rich stellar populations, higher rates of SF, and more metal rich gas. In general, the evolution of galaxies is governed by an inside-out growth during most of their life-time.

This evolution is verified for galaxies with stellar mass $M_* > 10^{9.5} M_\odot$. Below that mass most of the regions at any galactocentric distance are still in the rising phase of the SFHs, and therefore their chemical enrichment is slightly different, presenting flatter oxygen abundance gradients and even inverse stellar metallicity gradients. If this evolution is scaled towards higher-redshifts for more massive galaxies, it may indicate that the very early phase of the evolution of galaxies had an outside-in growth phase, that is shorter in massive galaxies, and has left almost no trace in the current fossil record. It is maybe possible that the outer regions of massive galaxies are still in this evolutionary phase, which may explain the flattening of some observed gradients in external regions of galaxies. I speculate here that the transition happens in the regime in which the infalling gas is of the same order as the original reservoir, which keeps the SFHs in a continuous (but smooth) rising phase.

The lack of (molecular) gas is the main driver for halting the SF activity, triggering a quenching that also evolves from the inside-out. In other words, the central regions of more massive galaxies, that have followed the sharper SFHs, exhaust the cold gas earlier than the outer regions of less massive ones. In addition, there is a decline in the star-formation efficiency, related to dynamical effects (i.e., a shift from a pure SK-law). It may well be that AGN feedback is the main driver for the absence of the SF fuel, either due to physical removal or by heating beyond the cooling time-scales. However, the dynamical effects introduced by the bulge dynamics seem to maintain the effects of the quenching for longer periods.

One of the main outcomes of large explorations of galaxy properties using IFS is that most galaxies present many different ionization processes at different locations. Thus, we should consider and study ionization as a local process. A fraction of galaxies may present AGN activity that could ionize (mostly) the central regions. But this does not preclude them for presenting star-formation activity in the disk, which produces a different kind of ionization. Central outflows could be observed in galaxies hosting an AGN or galaxies with strong nuclear SF activity. Even more, it is now clear that LINER-like emission is not dominated by weak-AGNs, as commonly assumed for decades (although ionization by weak-AGNs may also be present in some galaxies). The most probable reason for this kind of ionization, observed as diffuse ionized gas, is the presence of sufficiently old stellar populations (older than 1.6 Gyr, on average). However, in the case of radio galaxies, shock ionization may be a significant contribution to the ionization (i.e. the so called Red Geysers). But they represent less than a 1% of the total number of galaxies. Finally, in a very few cases, collimated synchrotron radiation associated with radio-jets could be sufficiently energetic to ionize the ISM (e.g., 3C120, M87). Alltogether, the description of the ionization stage of a galaxy using only integrated properties (e.g., line ratios) is fundamentally wrong. It has a pure statistical meaning, and only if there is a single ionization process that clearly dominates over the remaining ones. A particular care should be taken in the interpretation of the classical diagnostic diagrams, which make little sense unless they are combined with the properties of the underlying continuum (stellar population mostly). If not, they may lead to fundamental mistakes.

Finally, despite recent advances, there are caveats to the emerging picture: (i) we have a limited knowledge of the atomic and molecular gas content at the same spatial scales explored using the most recent IFS-GS (thus, covering a wide range of integrated properties as stellar masses and/or morphologies). Despite the individual efforts on a handful of targets (e.g. Lin et al. 2017), or pioneering explorations in large samples (e.g. Davis et al. 2013, Bolatto et al. 2017), there is still a need for a comprehensive exploration of the HI and H2 distribution at a kiloparsec scale for samples of galaxies

already observed using IFS. Current instruments, like the VLA could easily make such exploration for the atomic gas for those samples at low redshifts (AMUSING++, CALIFA, and the lower redshift targets of the MaNGA and SAMI surveys). For the molecular gas, ALMA would be ideal, in particular considering that the field-of-view of this instrument match pretty well that of MUSE and the optical extension of the galaxies of some of the quoted IFS-GS (e.g., CALIFA, whose diameter selection match with the FoV of ALMA). In other cases, like MaNGA or SAMI, the FoV of ALMA is considerably larger and therefore there is no perfect match of the covered regime between both observations. The lack of this dataset limits our knowledge of the gas-to-stars duty-cycle and our understanding of the feedback and quenching processes; (ii) we still do not know the real nature of the scaling relations. So far, we know that they are verified at kiloparsec scale, and we also know that they break at lower scales. Star-formation and chemical enrichment are very local processes and at the scale of an individual H II region these scaling relations are clearly not verified. This indicates that they have a statistical nature, and are only verified at certain volumes and time-scales: (a) volumes in which the integrated molecular and stellar masses are big enough to average the physical processes; (b) time-scales sufficiently long to compensate the instant star-formation with the metal mixing and stellar feedback, in different locations within the area (or volume) considered. Thus, they are the result of physical processes that indeed do not verify those scaling relations. IFS-GS exploring galaxies at much smaller physical scales (like PHANGS Rosolowsky et al. 2019) may tackle this problem in the near future. Following this reasoning, the derived SFHs and ChEHs also have a statistical nature, reflecting the envelop evolution of more pseudo-stochastic processes. In other words, the SFHs at lower scales do not present the described patterns, being dominated by peaks of star-formation that reflect the single events observed as individual H II regions; (iii) we need to extend our explorations to different wavelength ranges to improve our understanding of the properties of the stellar populations and the ionized gas. In particular, the combination of UV and FIR data with the information provided by IFS seems to be a promising tool to improve our estimations of the resolved SFHs and ChEHs (following López Fernández et al. 2018). So far we are limited by the coarse spatial resolution of the data in these wavelength ranges; (iv) we lack of a detailed knowledge of the AGN feedback and its connection with the bulge growth to the extend that we could explain the quenching using simple causal connections. We do not know whether the effect is purely mechanical (gas removal) or thermal (gas heating), or a combination of both and to which extent. We do not know which frequency is required to sustain the quenching or if it is a single event process, sustained by other processes (like bulge-induced dynamical effects). Actually, we do not know which is the real mechanism that makes bulges grow in time in sufficient detail; (v) we need to extend our current IFS explorations to larger samples at higher redshifts in order to study the evolution of the observed quantities and to determine whether our inferences based on the fossil records are compatible with observations. This would require new instruments still not foreseen or those installed in new facilities (like the IFS at the James Webb Space Telescope); finally, (vi) an effort should be made to develop detailed hydrodynamical and N-body simulations, with more precise recipes of the feedback, to a resolution good enough to compare with the current and future dataset. Little has been done to reproduce simultaneously the spatially-resolved and integrated scaling relations observed in galaxies using simulations to the extend that we can understand better the physical processes (following e.g., Trayford & Schaye 2019).

In summary, the most recent results based (mainly) on IFS-GS data and their combination with spatial resolved information of the cold gas content, have improved our understanding of the interconnections between star-formation, chemical enrichment and stellar evolution in general. New patterns and scaling relations have been uncovered, in particular at kiloparsec scales. In addition, previously known ones have been reinterpreted, mostly global scaling relations. However, there is still a vast number of unsolved problems that would require new data, new techniques, and a deeper inter-exchange

and cross-talk between observational and theoretical studies. As frequently happens in any branch of knowledge, new answers have lead to new questions that will require further explorations in the upcoming years.

SUMMARY POINTS

1. Summary point 1. Evolution of galaxies is governed by local properties but affected by global ones. Most scaling relations (like SK-law, MZR and SFMS) have local/resolved counterparts verified at kiloparsec scales, from which the global ones are integrated versions.
2. Summary point 2. Not all global relations are verified at local scales for all galaxy types and at any stellar masses (e.g., stellar MZR).
3. Summary point 3. Local scaling relations (and the lack of them) are a consequence of the narrow range of depletion times and the similarities of the local SFHs at fixed galactocentric distances of galaxies of similar final stellar mass, together with a chemical enrichment dominated by local processes.
4. Summary point 4. Radial gradients are a consequence of the local relations and the initial radial distribution of gas following the gravitational potential.
5. Summary point 5. Deviations from local relations (and gradients) are either (i) associated with dynamical and mixing processes, together with local exchange of gas (inflows, outflows, fountains), or (ii) described by diffrences in t_{dep} or the local SFHs among galaxy types.
6. Summary point 6. Ionization is a local process, that may be driven by different physical processes, and it cannot be clearly understood using purely integrated quantities.
7. Summary point 7. The dominant ionization in a certain location in a galaxy is mostly dictated by the properties of the underlying stellar population (that are connected with those of the ionized gas).

FUTURE ISSUES

1. Future issue 1. How the stellar and ionized gas properties connect with those of the cold gas (atomic and molecular) at kiloparsec scales? We require HI and H2 explorations at similar physical scales of current IFS-GS on large and statistically significant samples of galaxies already covered by those surveys.
2. Future issue 2. At which scales local relations are still verified? What this tell us about their nature? Are those statistical laws? IFS-GS expand to a smaller physical scales.
3. Future issue 3. IFS-GS should expand towards larger samples and at higher redshifts to constrain even more the evolutionary paths already uncovered by recent surveys. Covering lower mass ranges will be also fundamental.
4. Future issue 4. We need to refine our methods to recover the SFHs and ChEHs. Spatially-resolved spectroscopic information should be complemented with multiwavelength information at similar scales (that would require new UV and FIR explorers).
5. Future issue 5. Data at higher spectral resolution, deeper, and on wider wavelength ranges are required to use fainter emission lines to obtain precise information on the ionization conditions and the chemical composition of the gas.
6. Future issue 6. Which is the real quenching mechanism? Mergers? AGNs? stabilization? The involved mechanisms, in particular AGN feedback, should be understood in much more detail to be constrained better observationally.

7. Future issue 7. Larger efforts in detailed hydrodynamical and N-body simulations at kiloparsec and sub-kiloparsec scales are required to understand in detail the local/resolved scaling relations.

A. Integral Field Spectroscopy Galaxy Surveys

This review is focused in the recent results on the spatial resolved properties of galaxies derived using mostly Integral field spectroscopy (IFS). IFS is the technique that allows us to obtain simultaneously several spectra (within a defined field-of-view, FoV) of a quasi-continuous region in the sky. So, the final data, after reduction, consist either of a spatially continuous distribution of spectra (3D cube), or a set of individual spectra arranged across the FoV in certain fixed positions. It is beyond the scope of this review to enter in the details of the IFS technique, to explain the differences between the several Integral Field Units (IFUs), and to explain the data acquisition, reduction and analysis of this particular type of data. For these details I refer to Bershady (2009), and more extensively to the book published by R. Bacon (Optical 3D-Spectroscopy for Astronomy). I include in this review a brief description of the technique since most of the reviewed results are based on IFS.

IFS is not a totally new technique, with early experiments already presented in the 80's (e.g. Vanderriest et al. 1987). For years it was used to explore in detail the spatially resolved spectroscopic properties of a single object (or a handful of them). In the particular case of the study of galaxy properties, the stellar and gas kinematics, together with the exploration of ionization conditions in different regions, were more frequent uses of this technique (e.g. García-Lorenzo et al. 1997). The computational complexity of the data reduction and analysis hampered the development of IFS as common-user technique for decades, excluding its use for large samples of galaxies. Collective efforts (like the Euro3D RTN, Roth 2006), inspiring small-group initiatives (like the SAURON project, Bacon et al. 2001), and the increase of the computational capabilities along the years, allowed the implementation of IFS as a common-user technique and extended its use as a survey mode tool.

The SAURON project is usually considered the first attempt to perform an IFS galaxy survey (de Zeeuw et al. 2002). It explored the central regions of a representative sample of 72 early-type galaxies (E/S0/Sa) in the nearby universe (<42 Mpc) (de Zeeuw et al. 2002). The path opened by this project was continued by Atlas3D (Cappellari et al. 2011), the real first IFS-GS. It uses the same instrument as SAURON to study the central regions (R< 1.5Re) of a volume-limited sample of 260 galaxies of the same morphological type and at the same cosmological distances. Both projects explored mostly the properties of the stellar populations in early-type and bulges of early-spirals (e.g. Emsellem et al. 2004, Ganda et al. 2006), studying their dynamics, stellar composition, and the ionized gas properties (e.g. Kuntschner et al. 2010, Sarzi et al. 2010). Most of the results from both surveys were recently reviewed by Cappellari (2016).

The exploration of late type galaxies by IFS-GS started later. One major problem that delayed these studies was the presence of ionized gas along the disk of these objects. This involves an additional technical complication since it is required to separate the stellar and gas components in the analysis (e.g. Sánchez-Blázquez et al. 2011). Pioneering projects in the exploration of spiral-galaxies by IFS surveys were (i) the Disk Mass Survey (DMS, Bershady et al. 2010); (ii) the PINGS survey (Rosales-Ortega et al. 2010); (iii) the VENGA project (Blanc et al. 2010); and (iv) the CALIFA pilot survey (Mármol-Queraltó et al. 2011). Most of them were focused on the study of the ionized gas, and, in some cases, of the stellar populations, more than on the stellar/gas dynamics. I do not discuss in here explorations at high-redshift that are beyond the scope of this review.
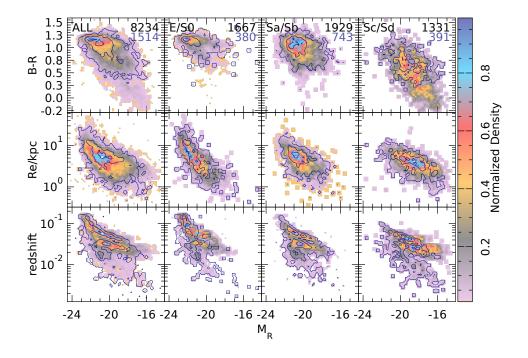
Table 1 Summary of the main properties of different IFS-GS

Parameter	MaNGA	SAMI	CALIFA	AMUSING++
Current sample size	6850	2400	974	540
Selection	M_* flat distribution	Volume limited	Diameter	Compilation
Redshift range	0.01-0.15	0.01-0.1	0.005-0.03	0.001-0.1
Mean redshift	0.03	0.04	0.015	0.017
Coverage	1.5 R_e (2/3), 2.5 R_e (1/3)	~1 R_e	>2.5 R_e	>2 R_e
S/N at $1r_e$ per spaxel	20	10	50	5
S/N at $1r_e$ per arcsec	40	20	50	25
Wavelength range (Å)	3600-10300	3700-5700/6250-7350	3700-7500	4650-9300
Original sampling elements	3×127^a	$n\times61^b$	3×331	90,000
Spectral resolution (σ)	80 km/s	75/28 km/s	85/150 km/s	40 km/s
Spatial resolution (FWHM)	2.5″	2.3″	2.5″	~0.7″
Physical spatial res. (kpc)	2.5 [0.5,6.5]	2.2 [0.4,4.6]	0.8 [0.3,1.5]	0.3 [0.1,1.3]
Telescope size	2.5m	3.6m	3.5m	8.2m
Gal. in sample	4655	910	2222	447
Gal. with morphology	2796	910	1062	343
Gal. in *resolved* sample	728	534	0^c	256

[a] This corresponds to the largest MaNGA bundle. Each MaNGA plate provides with 17 bundles of different amount of fibers: 2x19; 4x37; 4x61; 2x91; 5x127. [b] The dithering scheme in SAMI is repeated until a certain S/N is reached. Therefore the number of independent sampling elements is variable target to target. [c] Excluded due to the FoV of the SAMI IFU.

None of those pioneering surveys explored a wide range of galaxy properties, including all morphological types and/or covering a wide mass/luminosity/color regime, and in an statistically large sample of galaxies (e.g., Atlas3D observed only E/S0 and red early-spirals). The first IFS-GS fully representative of the population of galaxies in the near universe was the CALIFA survey, started in 2010 (Sánchez et al. 2012a). Moreover, it was the first IFS-GS designed as a legacy survey, i.e., with the main and primary goal to deliver the data freely to the community, easily accessible, and fully documented. Soon after, there were started the two major on-going IFS-GS, following the same phylosophy: MaNGA (Bundy et al. 2015) and SAMI (Croom et al. 2012). It is beyond the scope of this review to make a detailed comparison between them (for a referencee read Sánchez 2015, Sánchez et al. 2017). I briefly discuss of their main properties, listed in Table 1. From them, it is appreciated that CALIFA offers the best compromise between spatial resolution, covered fraction of the galaxy extension, and number of sampled elements. However, this comes at a cost, sampling much lower number of galaxies than MaNGA (1/10th) and SAMI (1/3th). Thus, for detailed analysis of the spatial resolved properties CALIFA may present an advantage. However, for galaxy statistics, MaNGA is far more superior. It also offers a wider wavelength range and a slightly better spectral resolution. Finally, it is worth noticing that although SAMI offers the smaller FoV (and covered area of each galaxy), it has by far the highest spectral resolution (in the red wavelength range). Thus, for kinematics (in particular gas one) it provides with more precise estimations. In general the three IFS-GS are pretty complementary, compensating somehow the limitations and strengths of each other.

In addition to this three major IFS-GS I included in Tab. 1 a large compilation of IFS observations of galaxies in the nearby universe performed with MUSE (Bacon et al. 2010). This instrument is by far the IFS that offers the best compromise between spatial sampling, resolution, FoV, spectral resolution and collecting power. It presents the only drawback of a limited wavelength range in the blue optical range (cut at 4650Å), what strongly affects any analysis of the stellar populations at low redshift. The

Distribution colors ($B - R$, *top panels*), effective radii (*central panels*), and redshifts (*bottom panels*) along the R-band absolute magnitudes for the collection of galaxies with IFS observations used in this review. *Left hand panels* show the distribution for the full sample, and each consecutive panel from left to right show similar distributions segregated by morphology (with the morphology indicated in the top panels). Color-maps show the density distribution normalized to the peak density for the full compilation, while contours show the same distribution for the sub-sample of *well resolved* galaxies (see the text). Each contour includes a 90%, 50% and 10% of the points. Finally, the number of galaxies included panel is indicated in the top panels, in black for the full sample and in color for the *well resolved* one.

current compilation, named `AMUSING++` (Lopez-Coba et al. in prep.), involves a diameter selection ($1\,R_e <$ FoV $< 3R_e$) of galaxies included in the ESO archive corresponding to different projects (e.g., MAD, GASP, TIMER, PHANGS, and AMUSING, Erroz-Ferrer et al. 2019, Poggianti et al. 2017, Gadotti et al. 2019, Kreckel et al. 2017, Galbany et al. 2016). Two thirds of the objects are extracted from the `AMUSING` survey (PI: J. Anderson), that was already used in different studies (e.g. Sánchez et al. 2015a, Sánchez-Menguiano et al. 2016b, López-Cobá et al. 2017a, Sánchez-Menguiano et al. 2018, Galbany et al. 2018). It is by far the largest compilation of IFU data with the best possible spatial resolution. It was included here for completeness and to highlight what would be achieved in the near future when such new instruments would be used in a survey mode.

I compiled all the public available data from all those IFS-GS (and compilations) to reproduce the main results reviewed along this article (as indicated in Sec. 2). This compilation comprises a total number of 8234 galaxies (and datacubes). This way I expect to minimize the possible biases introduced by the particularities of sample selection and instrumental details of each IFS-GS. The number of galaxies corresponding to each survey included in this compilation are listed in Tab. 1. In addition, I obtained the morphological classification for 2/3rd of them, using public information by different sources (Hyperleda for MUSE, Walcher et al. 2014, Sánchez et al. 2018, Cortesse private

communications for SAMI). For the particular purpose of this review I selected the best resolved and sampled galaxies, as indicated in Sec. 2 (i.e., the *well resolved* sub-sample).

It is clear that the current compilation does not comprise a well defined sample of galaxies (in principle). However, it is broadly representative of the general population of galaxies in the considered redshift range, since it was created from samples that are indeed representatives themselves. Figure 20 shows the distribution of colors ($B - R$), effective radii and redshifts along the R-band absolute magnitudes for the full compilation of galaxies (and segregated by morphology). Features as the red-sequence (for E/S0) and the blue-cloud (for Sc/Sd) are nicely recovered. Indeed, the morphological distribution is similar to the one recovered by volume limited surveys, with a ~33% of early-type galaxies (E/S0), a ~40% of early-spirals (Sa/Sb) and a ~27% of late-spirals (Sc/Sd) (e.g. Bamford et al. 2009). The fraction of SFGs (~50%), RGs (~46%), and AGN hosts (~4%) is also consistent with the most recent estimations at the considered redshift range (e.g. Cano-Díaz et al. 2016, , and references therein). The distribution along the R_e-$M_{abs,R}$ plane follows the expected trends for both the full population and the different morphological types (e.g. Cappellari 2016). Finally, the redshift-$M_{abs,R}$ distribution (and the derived redshift-R_e one) resembles that of a diameter-selected sample. This may or may not be the primarily selection criteria of the different IFS-GS included in this compilation, but all of them seek that their targets fit somehow within the FoV of their IFUs. In this later diagram the two distinctive distributions correspond to the CALIFA/AMUSSING++ and the MaNGA/SAMI subsamples, that cover two clearly different redshift ranges in general (see Tab. 1).

Fig. 20 shows also the distributions for the *well resolved* sub-sample (defined in Sec. 2). In general it presents a similar distribution than the full compilation for the parameters analyzed here. The strongest difference is the cut at low-luminosity and blue-colors, that corresponds in general to the tail towards low-mass galaxies presents in the SAMI sample, not well covered by other IFS-GS (e.g. Sánchez et al. 2017). However, excluding dwarf galaxies (not included in the current review), the two samples cover a similar range of parameters. Moreover, both of them seem to be representative of the global population of galaxies in the nearby universe (at a first order). As expected, the number of galaxies in the considered compilation is clearly dominated by the publicly available data from the MaNGA IFS-GS (DR15, Aguado et al. 2019), comprising ~57% of them (Tab. 1). However, only half of them have publicly available morphology, and just ~15% fulfil our severe criteria for the *well resolved* sub-sample. These cuts exclude all the SAMI data too, since I impose a minimum galaxy size larger than the FoV of their IFU. These are somehow arbitrary criteria, aimed to recover just the best sampled and resolved IFS data, and to homogenize (somehow) the different datasets. They do not imply any judgement on the quality of the different IFS-GS datasets considering their different goals and scopes. Further details of the compilation and its main global properties would be provided elsewhere (Sánchez et al. in prep.).

B. Ionized gas: A practical classification scheme

Based on the different results discussed along this review I present the following practical classification scheme to distinguish between different kinds of ionizing sources, in particular for IFS data at ~1 kpc resolution:

H II region: a gas cloud composed mostly by hydrogen ionized by young and hot stars.

AGN: active galactic nucleus, a compact region in the center of a galaxy, powered by the gas accreation to a super-massive black hole, with a blue and hard ionizing spectrum.

- **A star-forming or H II region:** It would be a clumpy area (clustered) in a galaxy in which the ionized gas emission line ratios are below the Kewley et al. (2001) demarcation line in at least one of the classical diagnostic diagrams involving [O III/Hβ] vs. [N II]/Hα, [S II]/Hα or [O I/Hα], with EW(Hα) above 6Å, and with a fraction of young stars (*age < 100Myr*) in flux in the visual-band of at least a 4-10%.

S.F.Sánchez

- **An AGN ionized region:** It would be that central ionized region, clearly more intense than the diffuse ionized gas, in which the emission line ratios are above the Kewley et al. (2001) demarcation line in the three diagrams indicated before, and with EW(Hα) above 3Å. Below that limit it is not possible to determine whether the ionization is due to an AGN or to other processes. The line ratios decreases with respect to the center of the galaxy, and the flux decays at r^{-2} or faster (nor following the light surface-brightness of the continuum).
- **Diffuse gas ionized by old stars (HOLMES, post-AGBs):** It is that smooth ionized structure that follows the light distribution of the old stellar population in galaxies, presenting an EW(Hα) clearly below 3Å. The fraction of young stars for the underlying stellar population is never larger than a 4%. It does not present any clumpy or filamentary distribution. In the BPT diagram could be located covering the LINER-like region (or AGN locus) towards the location of metal-rich star-forming regions. It is present in galaxies with old stellar populations (massive, earlier types) or regions in galaxies with the same characteristics (bulges), and it shares the same kinematic structure as the old stellar population.
- **Diffuse gas due to photon-leaking by H II regions:** They are smooth ionized structures present in galaxies with young stellar populations (in general, low mass and late-type galaxies) or regions in galaxies with the same characteristics (disks), presenting an EW(Hα) below 3Å, with fraction of young stars never larger than a 4%. It shares the same location of classical H II regions in the diagnostic diagrams, and should be included in the photon budget to derive the SFR in galaxies. Its kinematics is not fundamentally different of that of the disk. In high spatial resolution data (10-100 pc) it may present some shells or bubble-like structures, not visible at kpc scales.
- **A high-velocity shock ionized region:** It would be a filamentary or biconical ionized gas structure, with an intensity stronger than that of the diffuse ionized gas, in which the emission line ratios are above the indicated demarcation line in the three diagrams and with an EW(Hα) above 3Å, that shows asymmetrical lines extended through the filamentary structure. It presents a clear increase of the considered line ratios (in particular [O I/Hα]) with the velocity dispersion and the distance from the source of the outflow (the central region in the case of star-forming or AGN host galaxies). AGN and star-forming driven outflows could be separated, in principle, using the demarcation line proposed by Bland-Hawthorn (1995).
- **A low-velocity shock ionized region:** It shares many of the characteristics of the diffuse gas ionized by old stars, and indeed it is considered by different authors as diffuse (e.g. Dopita et al. 1996, Monreal-Ibero et al. 2010). However, it presents a clear filamentary structure, and a velocity distribution not following the general rotational pattern of the galaxy. Recent proposed red-geysers most probably are ionized by this kind of process (Kehrig et al. 2012a, Cheung et al. 2016).

DIG: diffuse ionized gas, a low intensity and smooth gas spread through most of the optical extension of galaxies.

Red Geyser: elliptical galaxy with filamentary ionized gas most probably due to shocks, but not clearly related with high-speed outflows.

Other sources of ionization, like super-nova remnants or planetary nebulae, are in general not resolved at kiloparsec scales, and they are sources of contamination that may complicate the classification even more. Moreover, in many cases it is not easy to clearly define which kind of region is observed, when different types are on the same aperture/line of sight. For a recent review on the properties of the ISM and how to recover them from emission lines I refer to Kewley et al. (2019).

DISCLOSURE STATEMENT

The author is not aware of any affiliations, memberships, funding, or financial holdings that might be perceived as affecting the objectivity of this review.

ACKNOWLEDGMENTS

LITERATURE CITED

Abdurro'uf, Akiyama M. 2017. *MNRAS* 469:2806–2820

Aguado DS, Ahumada R, Almeida A, Anderson SF, Andrews BH, et al. 2019. *ApJS* 240:23

Alatalo K, Davis TA, Bureau M, Young LM, Blitz L, et al. 2013. *MNRAS* 432:1796–1844

Asari NV, Cid Fernandes R, Stasińska G, Torres-Papaqui JP, Mateus A, et al. 2007. *MNRAS* 381:263–279

Athanassoula E. 1992. *MNRAS* 259:345–364

Bacon R, Accardo M, Adjali L, Anwand H, Bauer S, et al. 2010. *The MUSE second-generation VLT instrument*. In *SPIE Conf. Series*, vol. 7735

Bacon R, Copin Y, Monnet G, Miller BW, Allington-Smith JR, et al. 2001. *MNRAS* 326:23–35

Bakos J, Trujillo I, Pohlen M. 2008. *ApJL* 683:L103

Baldwin JA, Phillips MM, Terlevich R. 1981. *PASP* 93:5–19

Bamford SP, Nichol RC, Baldry IK, Land K, Lintott CJ, et al. 2009. *MNRAS* 393:1324–1352

Barrera-Ballesteros JK, Heckman T, Sánchez SF, Zakamska NL, Cleary J, et al. 2018. *ApJ* 852:74

Barrera-Ballesteros JK, Heckman TM, Zhu GB, Zakamska NL, Sánchez SF, et al. 2016. *MNRAS* 463:2513–2522

Barrera-Ballesteros JK, Sánchez SF, Heckman T, Blanc GA, The MaNGA Team. 2017. *ApJ* 844:80

Belfiore F, Maiolino R, Bothwell M. 2016. *MNRAS* 455:1218–1236

Belfiore F, Maiolino R, Bundy K, Masters K, Bershady M, et al. 2017a. *ArXiv e-prints*

Belfiore F, Maiolino R, Maraston C, Emsellem E, Bershady MA, et al. 2017b. *MNRAS* 466:2570–2589

Belfiore F, Maiolino R, Tremonti C, Sánchez SF, Bundy K, et al. 2017c. *MNRAS* 469:151–170

Belfiore F, Vincenzo F, Maiolino wR, Matteucci F. 2019a. *MNRAS*

Belfiore F, Westfall KB, Schaefer A, Cappellari M, Ji X, et al. 2019b. *arXiv e-prints* :arXiv:1901.00866

Bell EF, de Jong RS. 2001. *ApJ* 550:212–229

Bell EF, McIntosh DH, Barden M, Wolf C, Caldwell JAR, et al. 2004. *ApJL* 600:L11–L14

Bell EF, McIntosh DH, Katz N, Weinberg MD. 2003. *ApJS* 149:289–312

Bell EF, Phleps S, Somerville RS, Wolf C, Borch A, Meisenheimer K. 2006. *ApJ* 652:270–276

Belley J, Roy JR. 1992. *ApJS* 78:61–85

Belli S, Genzel R, Förster Schreiber NM, Wisnioski E, Wilman DJ, et al. 2017. *ApJL* 841:L6

Bershady MA. 2009. *arXiv e-prints* :arXiv:0910.0167

Bershady MA, Verheijen MAW, Swaters RA, Andersen DR, Westfall KB, Martinsson T. 2010. *ApJ* 716:198–233

Bigiel F, Leroy A, Walter F, Brinks E, de Blok WJG, et al. 2008. *AJ* 136:2846–2871

Binette L, Magris CG, Stasińska G, Bruzual AG. 1994. *A&A* 292:13–19

Bitsakis T, Dultzin D, Ciesla L, Díaz-Santos T, Appleton PN, et al. 2016. *MNRAS* 459:957–970

Blanc GA, Gebhardt K, Heiderman A, Evans II NJ, Jogee S, et al. 2010. *The VIRUS-P Exploration of Nearby Galaxies (VENGA): Survey Design and First Results*. In *Astronomical Society of the Pacific Conference Series*, ed. L. M. Stanford, J. D. Green, L. Hao, & Y. Mao, vol. 432 of *Astronomical Society of the Pacific Conference Series*

Bland-Hawthorn J. 1995. *PASA* 12:190

Blanton MR, Hogg DW, Bahcall NA, Brinkmann J, Britton M, et al. 2003. *ApJ* 592:819–838

Blanton MR, Moustakas J. 2009. *ARAA* 47:159–210

Boissier S, Prantzos N. 1999. *MNRAS* 307:857–876

Bolatto AD, Leroy AK, Rosolowsky E, Walter F, Blitz L. 2008. *ApJ* 686:948–965

Bolatto AD, Wolfire M, Leroy AK. 2013. *ARAA* 51:207–268

Bolatto AD, Wong T, Utomo D, Blitz L, Vogel SN, et al. 2017. *ApJ* 846:159

Bonnell IA, Bate MR, Zinnecker H. 1998. *MNRAS* 298:93–102

Boone F, Baker AJ, Schinnerer E, Combes F, García-Burillo S, et al. 2007. *Astronomy and Astrophysics* 471:113–125

Bresolin F. 2017. *Metallicities in the Outer Regions of Spiral Galaxies*. In *Outskirts of Galaxies*, eds. JH Knapen, JC Lee, A Gil de Paz, vol. 434 of *Astrophysics and Space Science Library*

Bresolin F. 2019. *Monthly Notices of the Royal Astronomical Society* 488:3826–3843

Bresolin F, Kennicutt RC. 2015. *MNRAS* 454:3664–3673

Brinchmann J, Charlot S, White SDM, Tremonti C, Kauffmann G, et al. 2004. *MNRAS* 351:1151–1179

Bundy K, Bershady MA, Law DR, Yan R, Drory N, et al. 2015. *ApJ* 798:7

Calette AR, Avila-Reese V, Rodríguez-Puebla A, Hernández-Toledo H, Papastergis E. 2018. *RMxAA* 54:443–483

Cano-Díaz M, Ávila-Reese V, Sánchez SF, Hernández-Toledo HM, Rodríguez-Puebla A, et al. 2019. *MNRAS* :1830

Cano-Díaz M, Sánchez SF, Zibetti S, Ascasibar Y, Bland-Hawthorn J, et al. 2016. *ApJL* 821:L26

Cappellari M. 2016. *ARAA* 54:597–665

Cappellari M, Emsellem E, Krajnović D, McDermid RM, Scott N, et al. 2011. *MNRAS* 413:813–836

Carigi L, Peimbert M, Peimbert A. 2019. *ApJ* 873:107

Casado J, Ascasibar Y, Gavilán M, Terlevich R, Terlevich E, et al. 2015. *MNRAS* 451:888–903

Catalán-Torrecilla C, Gil de Paz A, Castillo-Morales A, Iglesias-Páramo J, Sánchez SF, et al. 2015. *A&A* 584:A87

Cheung E, Bundy K, Cappellari M, Peirani S, Rujopakarn W, et al. 2016. *Nature* 533:504–508

Cid Fernandes R, González Delgado RM, García Benito R, Pérez E, de Amorim AL, et al. 2014. *A&A* 561:A130

Cid Fernandes R, Mateus A, Sodré L, Stasinska G, Gomes JM. 2011. STARLIGHT: Spectral Synthesis Code. Astrophysics Source Code Library

Cid Fernandes R, Pérez E, García Benito R, González Delgado RM, de Amorim AL, et al. 2013. *A&A* 557:A86

Cid Fernandes R, Stasińska G, Schlickmann MS, Mateus A, Vale Asari N, et al. 2010. *MNRAS* 403:1036–1053

Coccato L, Gerhard O, Arnaboldi M. 2010. *MNRAS* 407:L26–L30

Colombo D, Kalinova V, Utomo D, Rosolowsky E, Bolatto AD, et al. 2018. *MNRAS* 475:1791–1808

Comte G. 1975. *A&A* 39:197

Conroy C. 2013. *ARAA* 51:393–455

Courteau S, Cappellari M, de Jong RS, Dutton AA, Emsellem E, et al. 2014. *Reviews of Modern Physics* 86:47–119

Courteau S, de Jong RS, Broeils AH. 1996. *ApJL* 457:L73

Cresci G, Mannucci F, Curti M. 2019. *A&A* 627:A42

Croom SM, Lawrence JS, Bland-Hawthorn J, Bryant JJ, Fogarty L, et al. 2012. *MNRAS* 421:872–893

Croton DJ, Springel V, White SDM, De Lucia G, Frenk CS, et al. 2006. *MNRAS* 365:11–28

Daddi E, Dickinson M, Morrison G, Chary R, Cimatti A, et al. 2007. *ApJ* 670:156–172

Daddi E, Elbaz D, Walter F, Bournaud F, Salmi F, et al. 2010. *ApJL* 714:L118–L122

Davé R, Finlator K, Oppenheimer BD. 2011. *MNRAS* 416:1354–1376

Davies RL, Kewley LJ, Ho IT, Dopita MA. 2014. *MNRAS* 444:3961–3974

Davis TA, Alatalo K, Bureau M, Cappellari M, Scott N, et al. 2013. *MNRAS* 429:534–555

de Amorim AL, García-Benito R, Cid Fernandes R, Cortijo-Ferrero C, González Delgado RM, et al. 2017. *MNRAS* 471:3727–3752

de La Rosa IG, La Barbera F, Ferreras I, de Carvalho RR. 2011. *MNRAS* 418:L74–L78

de los Reyes MAC, Kennicutt Robert C. J. 2019. *ApJ* 872:16

de Vaucouleurs G. 1959. *Handbuch der Physik* 53:311

de Zeeuw PT, Bureau M, Emsellem E, Bacon R, Carollo CM, et al. 2002. *MNRAS* 329:513–530

Dey B, Rosolowsky E, Cao Y, Bolatto A, Sanchez SF, et al. 2019. *MNRAS* 488:1926–1940

Di Matteo P, Haywood M, Combes F, Semelin B, Snaith ON. 2013. *A&A* 553:A102

Diaz AI. 1989. *Abundance gradients in disc galaxies and chemical evolution models*. In *Evolutionary Phenomena in Galaxies*, ed. J. E. Beckman & B. E. J. Pagel

Dopita MA, Koratkar AP, Evans IN, Allen M, Bicknell GV, et al. 1996. *Shock Excitation of LINERs*. In *The Physics of Liners in View of Recent Observations*, eds. M Eracleous, A Koratkar, C Leitherer, L Ho, vol. 103 of *Astronomical Society of the Pacific Conference Series*

Driver SP, Andrews SK, da Cunha E, Davies LJ, Lagos C, et al. 2017. *ArXiv e-prints*

Driver SP, Norberg P, Baldry IK, Bamford SP, Hopkins AM, et al. 2009. *Astronomy and Geophysics* 50:5.12–5.19

Drory N, Fisher DB. 2007. *The Astrophysical Journal* 664:640–649

Elbaz D, Daddi E, Le Borgne D, Dickinson M, Alexander DM, et al. 2007. *A&A* 468:33–48

Ellison SL, Patton DR, Simard L, McConnachie AW. 2008. *ApJL* 672:L107–L110

Ellison SL, Sánchez SF, Ibarra-Medel H, Antonio B, Mendel JT, Barrera-Ballesteros J. 2018. *MNRAS* 474:2039–2054

Elmegreen BG. 1997. *Theory of Starbursts in Nuclear Rings*. In *Revista Mexicana de Astronomia y Astrofisica Conference Series*, eds. J Franco, R Terlevich, A Serrano, vol. 6 of *Revista Mexicana de Astronomia y Astrofisica, vol. 27*

Elmegreen DM, Elmegreen BG, Ravindranath S, Coe DA. 2007. *ApJ* 658:763–777

Emsellem E, Cappellari M, Peletier RF, McDermid RM, Bacon R, et al. 2004. *MNRAS* 352:721–743

Erb DK. 2008. *ApJ* 674:151–156

Erb DK, Shapley AE, Pettini M, Steidel CC, Reddy NA, Adelberger KL. 2006. *ApJ* 644:813–828

Erroz-Ferrer S, Carollo CM, den Brok M, Onodera M, Brinchmann J, et al. 2019. *MNRAS* :200

Esteban C, García-Rojas J. 2018. *MNRAS*

Faber S. 1977. In *The Evolution of Galaxies and Stellar Populations*, ed. BMTRB Larson

Faber SM, Willmer CNA, Wolf C, Koo DC, Weiner BJ, et al. 2007. *ApJ* 665:265–294

Fabian AC. 2012. *ARAA* 50:455–489

Flores-Fajardo N, Morisset C, Stasińska G, Binette L. 2011. *MNRAS* 415:2182–2192

Freeman KC. 1970. *ApJ* 160:811

Gadotti DA, Sánchez-Blázquez P, Falcón-Barroso J, Husemann B, Seidel MK, et al. 2019. *MNRAS* 482:506–529

Galbany L, Anderson JP, Rosales-Ortega FF, Kuncarayakti H, Krühler T, et al. 2016. *MNRAS* 455:4087–4099

Galbany L, Collett TE, Méndez-Abreu J, Sánchez SF, Anderson JP, Kuncarayakti H. 2018. *MNRAS* 479:262–274

Gallazzi A, Brinchmann J, Charlot S, White SDM. 2008. *MNRAS* 383:1439–1458

Gallazzi A, Charlot S, Brinchmann J, White SDM, Tremonti CA. 2005. *MNRAS* 362:41–58

Ganda K, Falcón-Barroso J, Peletier RF, Cappellari M, Emsellem E, et al. 2006. *Mon. Not. R. Astron. Soc.* 367:46

García-Benito R, González Delgado RM, Pérez E, Cid Fernandes R, Cortijo-Ferrero C, et al. 2017. *A&A* 608:A27

García-Benito R, González Delgado RM, Pérez E, Cid Fernandes R, Sánchez SF, de Amorim AL. 2019. *A&A* 621:A120

García-Lorenzo B, Mediavilla E, Arribas S, del Burgo C. 1997. *ApJ* 483:L99–L102

Garnett DR. 2002. *ApJ* 581:1019–1031

Gavazzi G, Consolandi G, Dotti M, Fanali R, Fossati M, et al. 2015. *A&A* 580:A116

Genzel R, Tacconi LJ, Gracia-Carpio J, Sternberg A, Cooper MC, et al. 2010. *MNRAS* 407:2091–2108

Goddard D, Thomas D, Maraston C, Westfall K, Etherington J, et al. 2017. *MNRAS* 466:4731–4758

Gomes JM, Papaderos P, Kehrig C, Vílchez JM, Lehnert MD, et al. 2016a. *A&A* 588:A68

Gomes JM, Papaderos P, Vílchez JM, Kehrig C, Iglesias-Páramo J, et al. 2016b. *A&A* 585:A92

González J. 1994. In *Ph.D. Thesis, Univ. California, Santa Cruz (G93)*

González Delgado RM, Cid Fernandes R, García-Benito R, Pérez E, de Amorim AL, et al. 2014a. *ApJL* 791:L16

González Delgado RM, Cid Fernandes R, Pérez E, García-Benito R, López Fernández R, et al. 2016. *A&A* 590:A44

González Delgado RM, García-Benito R, Pérez E, Cid Fernandes R, de Amorim AL, et al. 2015. *A&A* 581:A103

González Delgado RM, Pérez E, Cid Fernandes R, et al. 2014b. *A&A* 562:A47

González Delgado RM, Pérez E, Cid Fernandes R, García-Benito R, López Fernández R, et al. 2017. *A&A* 607:A128

Graham MT, Cappellari M, Li H, Mao S, Bershady MA, et al. 2018. *MNRAS* 477:4711–4737

Grand RJJ, Springel V, Kawata D, Minchev I, Sánchez-Blázquez P, et al. 2016. *MNRAS* 460:L94–L98

Heavens A, Panter B, Jimenez R, Dunlop J. 2004. *Nature* 428:625–627

Heckman TM, Armus L, Miley GK. 1990. *ApJS* 74:833–868

Henriques BMB, White SDM, Lilly SJ, Bell EF, Bluck AFL, Terrazas BA. 2019. *MNRAS* 485:3446–3456

Henry A, Scarlata C, Domínguez A, Malkan M, Martin CL, et al. 2013. *ApJL* 776:L27

Ho IT, Kewley LJ, Dopita MA, Medling AM, Allen JT, et al. 2014. *MNRAS* 444:3894–3910

Ho IT, Medling AM, Groves B, Rich JA, Rupke DSN, et al. 2016. *Astrophysics and Space Science* 361:280

Ho IT, Meidt SE, Kudritzki RP, Groves BA, Seibert M, et al. 2018. *A&A* 618:A64

Ho IT, Seibert M, Meidt SE, Kudritzki RP, Kobayashi C, et al. 2017. *ApJ* 846:39

Hopkins PF, Cox TJ, Younger JD, Hernquist L. 2009. *ApJ* 691:1168–1201

Hsieh BC, Lin L, Lin JH, Pan HA, Hsu CH, et al. 2017. *ApJL* 851:L24

Hubble E. 1936. *ApJ* 84:517

Hubble EP. 1926. *ApJ* 63

Hughes A, Wong T, Ott J, Muller E, Pineda JL, et al. 2010. *MNRAS* 406:2065–2086

Husemann B, Jahnke K, Sánchez SF, Wisotzki L, Nugroho D, et al. 2014. *MNRAS* 443:755–783

Husemann B, Sánchez SF, Wisotzki L, Jahnke K, Kupko D, et al. 2010. *A&A* 519:A115+

Hwang HC, Barrera-Ballesteros JK, Heckman TM, Rowlands K, Lin L, et al. 2018. *arXiv e-prints*

Ibarra-Medel HJ, Avila-Reese V, Sánchez SF, González-Samaniego A, Rodríguez-Puebla A. 2019. *MNRAS* 483:4525–4550

Ibarra-Medel HJ, Sánchez SF, Avila-Reese V, Hernández-Toledo HM, González JJ, et al. 2016. *MNRAS* 463:2799–2818

Jarvis BJ. 1990. *Astronomy and Astrophysics* 240:L8

Jogee S, Scoville N, Kenney JDP. 2005. *ApJ* 630:837–863

Kauffmann G, Heckman TM, Tremonti C, Brinchmann J, Charlot S, et al. 2003. *MNRAS* 346:1055–1077

Kehrig C, Monreal-Ibero A, Papaderos P, Vílchez JM, Gomes JM, et al. 2012a. *A&A* 540:A11

Kehrig C, Monreal-Ibero A, Papaderos P, Vílchez JM, Gomes JM, et al. 2012b. *A&A* 540:A11

Kennicutt RC, Evans NJ. 2012. *ARAA* 50:531–608

Kennicutt Jr. RC. 1998a. *ARAA* 36:189–232

Kennicutt Jr. RC. 1998b. *ApJ* 498:541–552

Kennicutt Jr. RC, Calzetti D, Walter F, Helou G, Hollenbach DJ, et al. 2007. *ApJ*

Kennicutt Jr. RC, Keel WC, Blaha CA. 1989. *AJ* 97:1022–1035

Kewley LJ, Dopita MA, Sutherland RS, Heisler CA, Trevena J. 2001. *ApJ* 556:121–140

Kewley LJ, Ellison SL. 2008. *ApJ* 681:1183–1204

Kewley LJ, Nicholls DC, Sutherland RS. 2019. *Annual Review of Astronomy and Astrophysics* 57:511–570

Knapen JH, Comerón S, Seidel MK. 2019. *Astronomy and Astrophysics* 621:L5

Koleva M, Prugniel P, De Rijcke S, Zeilinger WW. 2011. *MNRAS* 417:1643–1671

Kormendy J, Ho LC. 2013. *ARAA* 51:511–653

Kreckel K, Groves B, Bigiel F, Blanc GA, Kruijssen JMD, et al. 2017. *ApJ* 834:174

Kruijssen JMD, Longmore SN. 2014. *MNRAS* 439:3239–3252

Kruijssen JMD, Schruba A, Chevance M, Longmore SN, Hygate AePS, et al. 2019. *Nature* 569:519–522

Krumholz MR, Dekel A, McKee CF. 2012. *ApJ* 745:69

Kuntschner H. 2015. *ATLAS*^{3D} *Stellar Population Gradients*. In *Galaxy Masses as Constraints of Formation Models*, eds. M Cappellari, S Courteau, vol. 311 of *IAU Symposium*

Kuntschner H, Emsellem E, Bacon R, Cappellari M, Davies RL, et al. 2010. *MNRAS* 408:97–132

Lacerda EAD, Cid Fernandes R, Couto GS, Stasińska G, García-Benito R, et al. 2018. *MNRAS* 474:3727–3739

Lara-López MA, Cepa J, Bongiovanni A, Pérez García AM, Ederoclite A, et al. 2010. *A&A* 521:L53

Leroy AK, Walter F, Brinks E, Bigiel F, de Blok WJG, et al. 2008. *AJ* 136:2782–2845

Leroy AK, Walter F, Sandstrom K, Schruba A, Munoz-Mateos JC, et al. 2013. *AJ* 146:19

Li C, Wang E, Lin L, Bershady MA, Bundy K, et al. 2015. *ApJ* 804:125

Li Y, Bresolin F, Kennicutt Jr. RC. 2013. *ApJ* 766:17

Lilly SJ, Carollo CM, Pipino A, Renzini A, Peng Y. 2013. *ApJ* 772:119

Lin L, Belfiore F, Pan HA, Bothwell MS, Hsieh PY, et al. 2017. *ApJ* 851:18

López-Cobá C, Sánchez SF, Bland -Hawthorn J, Moiseev AV, Cruz-González I, et al. 2019. *MNRAS* 482:4032–4056

López-Cobá C, Sánchez SF, Cruz-González I, Binette L, Galbany L, et al. 2017a. *ApJ* 850:L17

López-Cobá C, Sánchez SF, Moiseev AV, Oparin DV, Bitsakis T, et al. 2017b. *MNRAS* 467:4951–4964

López Fernández R, Cid Fernandes R, González Delgado RM, Vale Asari N, Pérez E, et al. 2016. *MNRAS* 458:184–199

López Fernández R, González Delgado RM, Pérez E, García-Benito R, Cid Fernandes R, et al. 2018. *A&A* 615:A27

Madau P, Dickinson M. 2014. *ARAA* 52:415–486

Madau P, Pozzetti L, Dickinson M. 1998. *ApJ* 498:106–116

Magorrian J, Tremaine S, Richstone D, Bender R, Bower G, et al. 1998. *AJ* 115:2285–2305

Maiolino R, Mannucci F. 2019. *The Astronomy and Astrophysics Review* 27:3

Maiolino R, Nagao T, Grazian A, Cocchia F, Marconi A, et al. 2008. *A&A* 488:463–479

Mannucci F, Cresci G, Maiolino R, Marconi A, Gnerucci A. 2010. *MNRAS* 408:2115–2127

Maragkoudakis A, Zezas A, Ashby MLN, Willner SP. 2016. *ArXiv e-prints*

Marino RA, Gil de Paz A, Sánchez SF, Sánchez-Blázquez P, Cardiel N, et al. 2016. *A&A* 585:A47

Marino RA, Rosales-Ortega FF, Sánchez SF, Gil de Paz A, Vílchez J, et al. 2013. *A&A* 559:A114

Mármol-Queraltó E, Sánchez SF, Marino RA, Mast D, Viironen K, et al. 2011. *A&A* 534:A8

Martig M, Bournaud F, Teyssier R, Dekel A. 2009. *ApJ* 707:250–267

Martin P, Roy JR. 1994. *ApJ* 424:599–614

Matteucci F, Francois P. 1989. *MNRAS* 239:885–904

McDermid RM, Alatalo K, Blitz L, Bournaud F, Bureau M, et al. 2015. *MNRAS* 448:3484–3513

McIntosh DH, Wagner C, Cooper A, Bell EF, Kereš D, et al. 2014. *MNRAS* 442:533–557

Medling AM, Cortese L, Croom SM, Green AW, Groves B, et al. 2018. *MNRAS* 475:5194–5214

Mehlert D, Thomas D, Saglia RP, Bender R, Wegner G. 2003. *A&A* 407:423–435

Méndez-Abreu J, Ruiz-Lara T, Sánchez-Menguiano L, de Lorenzo-Cáceres A, Costantin L, et al. 2017. *A&A* 598:A32

Minchev I, Famaey B, Quillen AC, Di Matteo P, Combes F, et al. 2012. *ArXiv e-prints*

Mollá M, Díaz AI. 2005. *MNRAS* 358:521–543

Monreal-Ibero A, Vílchez JM, Walsh JR, Muñoz-Tuñón C. 2010. *A&A* 517:A27

Moran SM, Heckman TM, Kauffmann G, Davé R, Catinella B, et al. 2012. *ApJ* 745:66

Morisset C, Delgado-Inglada G, Sánchez SF, Galbany L, García-Benito R, et al. 2016. *A&A* 594:A37

Moustakas J, Kennicutt Jr. RC. 2006. *ApJ* 651:155–166

Noeske KG, Faber SM, Weiner BJ, Koo DC, Primack JR, et al. 2007. *ApJL* 660:L47–L50

Osterbrock DE. 1989. *Astrophysics of gaseous nebulae and active galactic nuclei*. University Science Books

Oyarzun GA, Bundy K, Westfall KB, Belfiore F, Thomas D, et al. 2019. *arXiv e-prints* :arXiv:1906.05298

Pagel BEJ, Edmunds MG. 1981. *ARAA* 19:77–113

Pan HA, Lin L, Hsieh BC, Sánchez SF, Ibarra-Medel H, et al. 2018. *ApJ* 854:159

Panter B, Heavens AF, Jimenez R. 2003. *MNRAS* 343:1145–1154

Panter B, Jimenez R, Heavens AF, Charlot S. 2007. *MNRAS* 378:1550–1564

Panter B, Jimenez R, Heavens AF, Charlot S. 2008. *MNRAS* 391:1117–1126

Papaderos P, Gomes JM, Vílchez JM, Kehrig C, Lehnert MD, et al. 2013. *A&A* 555:L1

Peimbert M, Luridiana V, Peimbert A. 2007. *The Astrophysical Journal* 666:636–646

Peimbert M, Torres-Peimbert S, Rayo JF. 1978. *ApJ* 220:516–524

Peletier RF. 1989. *Elliptical Galaxies - Structure and Stellar Content*. Ph.D. thesis, , University of Groningen, The Netherlands, (1989)

Peletier RF, Davies RL, Illingworth GD, Davis LE, Cawson M. 1990. *AJ* 100:1091–1142

Peng Yj, Lilly SJ, Kovač K, Bolzonella M, Pozzetti L, et al. 2010. *ApJ* 721:193–221

Pérez E, Cid Fernandes R, González Delgado RM, García-Benito R, Sánchez SF, et al. 2013. *ApJL* 764:L1

Pérez-González PG, Rieke GH, Villar V, Barro G, Blaylock M, et al. 2008. *ApJ* 675:234–261

Pérez-Montero E. 2014. *MNRAS* 441:2663–2675

Pérez-Montero E. 2017. *PASP* 129:043001

Peterken TG, Merrifield MR, Aragón-Salamanca A, Drory N, Krawczyk CM, et al. 2018. *Nature Astronomy*

Pettini M, Pagel BEJ. 2004. *MNRAS* 348:L59–L63

Pilyugin LS, Grebel EK, Kniazev AY. 2014. *AJ* 147:131

Pilyugin LS, Thuan TX, Vílchez JM. 2007. *MNRAS* 376:353–360

Poetrodjojo H, Groves B, Kewley LJ, Medling AM, Sweet SM, et al. 2018. *MNRAS* 479:5235–5265

Poggianti BM, Moretti A, Gullieuszik M, Fritz J, Jaffé Y, et al. 2017. *ApJ* 844:48

Pozzetti L, Bolzonella M, Zucca E, Zamorani G, Lilly S, et al. 2010. *A&A* 523:A13

Rahman N, Bolatto AD, Xue R, Wong T, Leroy AK, et al. 2012. *ApJ* 745:183

Rawle TD, Smith RJ, Lucey JR. 2010. *MNRAS* 401:852–866

Rawle TD, Smith RJ, Lucey JR, Swinbank AM. 2008. *MNRAS* 389:1891–1904

Regan MW, Thornley MD, Helfer TT, Sheth K, Wong T, et al. 2001. *ApJ* 561:218–237

Renzini A, Peng Yj. 2015. *ApJL* 801:L29

Rodríguez-Puebla A, Primack JR, Behroozi P, Faber SM. 2016. *MNRAS* 455:2592–2606

Rosales-Ortega FF, Díaz AI, Kennicutt RC, Sánchez SF. 2011. *MNRAS* 415:2439–2474

Rosales-Ortega FF, Kennicutt RC, Sánchez SF, Díaz AI, Pasquali A, et al. 2010. *MNRAS* 405:735–758

Rosales-Ortega FF, Sánchez SF, Iglesias-Páramo J, Díaz AI, Vílchez JM, et al. 2012. *ApJL* 756:L31

Rosolowsky E, Schinnerer E, Leroy A, Pety J, Herrera C, et al. 2019. *Physics at High Angular resolution in Nearby Galaxies (PHANGS)*. In *American Astronomical Society Meeting Abstracts #233*, vol. 233 of *American Astronomical Society Meeting Abstracts*

Roth MM. 2006. *New Astronomy Review* 50:252–258

Roy JR, Walsh JR. 1997. *MNRAS* 288:715–725

Roy N, Bundy K, Cheung E, Rujopakarn W, Cappellari M, et al. 2018. *The Astrophysical Journal* 869:117

Ruiz-Lara T, Pérez I, Florido E, Sánchez-Blázquez P, Méndez-Abreu J, et al. 2016. *MNRAS* 456:L35–L39

Ruiz-Lara T, Pérez I, Florido E, Sánchez-Blázquez P, Méndez-Abreu J, et al. 2017. *A&A* 604:A4

Ryder SD. 1995. *ApJ* 444:610–631

Saintonge A, Catinella B, Cortese L, Genzel R, Giovanelli R, et al. 2016. *MNRAS* 462:1749–1756

Saintonge A, Catinella B, Tacconi LJ, Kauffmann G, Genzel R, et al. 2017. *ApJS* 233:22

Saintonge A, Kauffmann G, Kramer C, Tacconi LJ, Buchbender C, et al. 2011. *MNRAS* 415:32–60

Salim S, Lee JC, Davé R, Dickinson M. 2015. *ApJ* 808:25

Salim S, Lee JC, Ly C, Brinchmann J, Davé R, et al. 2014. *ApJ* 797:126

Salpeter EE. 1955. *ApJ* 121:161

Sánchez SF. 2015. *IFUs surveys, a panoramic view of galaxy evolution*. In *Galaxies in 3D across the Universe*, eds. BL Ziegler, F Combes, H Dannerbauer, M Verdugo, vol. 309 of *IAU Symposium*

Sánchez SF, Avila-Reese V, Hernandez-Toledo H, Cortes-Suárez E, Rodríguez-Puebla A, et al. 2018. *RMxAA* 54:217–260

Sánchez SF, Avila-Reese V, Rodríguez-Puebla A, Ibarra-Medel H, Calette R, et al. 2019a. *MNRAS* 482:1557–1586

Sánchez SF, Barrera-Ballesteros JK, López-Cobá C, Brough S, Bryant JJ, et al. 2019b. *MNRAS* 484:3042–3070

Sánchez SF, Barrera-Ballesteros JK, Sánchez-Menguiano L, Walcher CJ, Marino RA, et al. 2017. *MNRAS* 469:2121–2140

Sánchez SF, Galbany L, Pérez E, Sánchez-Blázquez P, Falcón-Barroso J, et al. 2015a. *A&A* 573:A105

Sánchez SF, García-Benito R, Zibetti S, Walcher CJ, Husemann B, et al. 2016a. *A&A* 594:A36

Sánchez SF, Jahnke K, Wisotzki L, McIntosh DH, Bell EF, et al. 2004. *ApJ* 614:586–606

Sánchez SF, Kennicutt RC, Gil de Paz A, van de Ven G, Vílchez JM, et al. 2012a. *A&A* 538:A8

Sánchez SF, Pérez E, Rosales-Ortega FF, Miralles-Caballero D, López-Sánchez AR, et al. 2015b. *A&A* 574:A47

Sánchez SF, Pérez E, Sánchez-Blázquez P, García-Benito R, Ibarra-Mede HJ, et al. 2016b. *RMxAA* 52:171–220

Sánchez SF, Pérez E, Sánchez-Blázquez P, González JJ, Rosález-Ortega FF, et al. 2016c. *RMxAA* 52:21–53

Sánchez SF, Rosales-Ortega FF, Iglesias-Páramo J, Mollá M, Barrera-Ballesteros J, et al. 2014. *A&A* 563:A49

Sánchez SF, Rosales-Ortega FF, Jungwiert B, Iglesias-Páramo J, Vílchez JM, et al. 2013. *A&A* 554:A58

Sánchez SF, Rosales-Ortega FF, Marino RA, Iglesias-Páramo J, Vílchez JM, et al. 2012b. *A&A* 546:A2

Sánchez SF, Sánchez-Menguiano L. 2017. *Integral Field Spectroscopy Surveys: Oxygen Abundance Gradients*. In *Revista Mexicana de Astronomia y Astrofisica Conference Series*, vol. 49

Sánchez Almeida J, Sánchez-Menguiano L. 2019. *ApJL* 878:L6

Sánchez-Blázquez P, Forbes DA, Strader J, Brodie J, Proctor R. 2007. *MNRAS* 377:759–786

Sánchez-Blázquez P, Ocvirk P, Gibson BK, Pérez I, Peletier RF. 2011. *MNRAS* 415:709–731

Sánchez-Blázquez P, Rosales-Ortega F, Diaz A, Sánchez SF. 2014a. *MNRAS* 437:1534–1548

Sánchez-Blázquez P, Rosales-Ortega FF, Méndez-Abreu J, Pérez I, Sánchez SF, et al. 2014b. *A&A* 570:A6

Sánchez-Menguiano L, Sánchez SF, Kawata D, Chemin L, Pérez I, et al. 2016a. *ApJL* 830:L40

Sánchez-Menguiano L, Sánchez SF, Pérez I, García-Benito R, Husemann B, et al. 2016b. *A&A* 587:A70

Sánchez-Menguiano L, Sánchez SF, Pérez I, Ruiz-Lara T, Galbany L, et al. 2018. *A&A* 609:A119

Sánchez-Menguiano L, Sánchez Almeida J, Muñoz-Tuñón C, Sánchez SF, Filho M, et al. 2019. *arXiv e-prints*

Sanders DB, Mirabel IF. 1996. *ARAA* 34:749

Sarzi M, Falcón-Barroso J, Davies RL, Bacon R, Bureau M, et al. 2006. *MNRAS* 366:1151–1200

Sarzi M, Shields JC, Schawinski K, Jeong H, Shapiro K, et al. 2010. *MNRAS* 402:2187–2210

Schawinski K, Urry CM, Simmons BD, Fortson L, Kaviraj S, et al. 2014. *MNRAS* 440:889–907

Schawinski K, Urry CM, Virani S, Coppi P, Bamford SP, et al. 2010. *ApJ* 711:284–302

Schiminovich D, Wyder TK, Martin DC, Johnson BD, Salim S, et al. 2007. *ApJS* 173:315–341

Schmidt M. 1959. *ApJ* 129:243

Schruba A, Kruijssen JMD, Leroy AK. 2019. *arXiv e-prints* :arXiv:1908.04306

Schruba A, Leroy AK, Walter F, Bigiel F, Brinks E, et al. 2011. *AJ* 142:37

Scott N, van de Sande J, Croom SM, Groves B, Owers MS, et al. 2018. *ArXiv e-prints*

Searle L. 1971. *ApJ* 168:327

Sersic JL. 1968. *Atlas de galaxias australes*

Shlosman I, Frank J, Begelman MC. 1989. *Nature* 338:45–47

Silk J. 1997. *ApJ* 481:703–709

Singh R, van de Ven G, Jahnke K, Lyubenova M, et al. 2013. *A&A* 558:A43

Speagle JS, Steinhardt CL, Capak PL, Silverman JD. 2014. *ApJS* 214:15

Spolaor M, Kobayashi C, Forbes DA, Couch WJ, Hau GKT. 2010. *MNRAS* 408:272–292

Stark DV, Bundy KA, Orr ME, Hopkins PF, Westfall K, et al. 2018. *MNRAS* 474:2323–2333

Stasińska G, Vale Asari N, Cid Fernandes R, Gomes JM, Schlickmann M, et al. 2008. *MNRAS* 391:L29–L33

Strateva I, Ivezić Ž, Knapp GR, Narayanan VK, Strauss MA, et al. 2001. *AJ* 122:1861–1874

Strömgren B. 1939. *ApJ* 89:526

Thilker DA, Bianchi L, Meurer G, Gil de Paz A, Boissier S, et al. 2007. *ApJS* 173:538–571

Thomas D, Maraston C, Bender R, Mendes de Oliveira C. 2005. *ApJ* 621:673–694

Thomas D, Maraston C, Schawinski K, Sarzi M, Silk J. 2010. *MNRAS* 404:1775–1789

Tissera PB, Scannapieco C, Beers TC, Carollo D. 2013. *MNRAS* 432:3391–3400

Torres-Papaqui JP, Coziol R, Andernach H, Ortega-Minakata RA, Neri-Larios DM, Plauchu-Frayn I. 2012. *RMxAA* 48:275–291

Tortora C, Napolitano NR, Cardone VF, Capaccioli M, Jetzer P, Molinaro R. 2010. *MNRAS* 407:144–162

Trayford JW, Schaye J. 2019. *MNRAS* 485:5715–5732

Tremonti CA, Heckman TM, Kauffmann G, Brinchmann J, Charlot S, et al. 2004. *ApJ* 613:898–913

Urry CM, Padovani P. 1995. *PASP* 107:803

Utomo D, Bolatto AD, Wong T, Ostriker EC, Blitz L, et al. 2017. *ArXiv e-prints*

Vale Asari N, Stasińska G, Cid Fernandes R, Gomes JM, Schlickmann M, et al. 2009. *MNRAS* 396:L71–L75

van de Sande J, Lagos CDP, Welker C, Bland-Hawthorn J, Schulze F, et al. 2019. *MNRAS* 484:869–891

Vanderriest C, Haddad B, Lemonnier JP. 1987. *Interaction Between Quasars and Galaxies - First Results from Bidimensional Spectrography with Silfid*. In *L'Activite dans les Galaxies*

Veilleux S, Cecil G, Bland-Hawthorn J. 2005. *ARAA* 43:769–826

Veilleux S, Osterbrock DE. 1987. *ApJS* 63:295–310

Vila-Costas MB, Edmunds MG. 1992. *MNRAS* 259:121–145

Vilchez JM, Esteban C. 1996. *MNRAS* 280:720–734

Vogt FPA, Pérez E, Dopita MA, Verdes-Montenegro L, Borthakur S. 2017. *A&A* 601:A61

Walcher CJ, Wisotzki L, Bekeraité S, Husemann B, Iglesias-Páramo J, et al. 2014. *A&A* 569:A1

Walcher J, Groves B, Budavári T, Dale D. 2011. *ApSS* 331:1–52

Weinberg DH, Andrews BH, Freudenburg J. 2017. *ApJ* 837:183

Wong T, Blitz L. 2002. *ApJ* 569:157–183

Worthey G. 1994. *ApJS* 95:107–149

Wuyts S, Förster Schreiber NM, Nelson EJ, van Dokkum PG, Brammer G, et al. 2013. *ApJ* 779:135

Yates RM, Kauffmann G, Guo Q. 2012. *MNRAS* 422:215–231

York DG, Adelman J, Anderson Jr. JE, Anderson SF, Annis J, et al. 2000. *AJ* 120:1579–1587

Young LM, Bureau M, Davis TA, Combes F, McDermid RM, et al. 2011. *MNRAS* 414:940–967

Zaritsky D, Kennicutt Jr. RC, Huchra JP. 1994. *ApJ* 420:87–109

Zheng Z, Wang H, Ge J, Mao S, Li C, et al. 2017. *MNRAS* 465:4572–4588

Zibetti S, Charlot S, Rix H. 2009. *MNRAS* 400:1181–1198

Zibetti S, Gallazzi AR, Ascasibar Y, Charlot S, Galbany L, et al. 2017. *ArXiv e-prints*

Zinchenko IA, Pilyugin LS, Grebel EK, Sánchez SF, Vílchez JM. 2016. *MNRAS* 462:2715–2733